

# 1

## Introduction

### 1.1 History of Scintillator Developments

A scintillator can convert radiation (alpha-ray, beta-ray, gamma-ray, X-ray, and neutron) into light (photon), and radiation detectors using scintillators and photo acceptance units have been used for various applications in medical, security, environmental, high-energy fields, etc. (Figure 1.1). Photo acceptance units such as photomultiplier tubes (PMT), photodiodes, and multi-pixel photon counters (MPPC) can convert light into electrical signals, which enables detection and measurement (count) of radiation using multi-channel analyzers.

In these applications, there are some required properties of scintillators, and the required performance that is considered important varies greatly depending on the type of application. Typical parameters considered important in scintillator crystals include light yield, energy resolution, decay time, density, effective atomic number, emission wavelength, and afterglow. Furthermore, mass productivity, chemical stability, crystal workability, radiation resistance, etc. are also important for commercial use. For example, high light yield, large density and effective atomic number, and short decay time are required in applications under gamma-ray irradiation with the short measurement time.

One of the most important characteristics of scintillators is the light yield, which is directly related to radiation detection sensitivity. For the emitted light in the scintillator under radiation to efficiently enter the photo acceptance unit, the scintillator must be transparent at the emission wavelength. Especially in the case of high-energy radiation such as gamma-ray, the scintillator becomes large enough to stop the radiation inside, so efficient extraction of the emitted light inside greatly affects the performance of the scintillator. Therefore, many scintillators have been utilized as single crystals with high transparency.

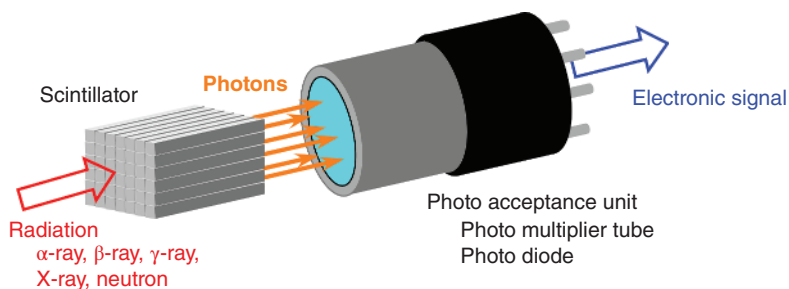


**Figure 1.1** Schematic diagram of scintillator and photo acceptance unit in radiation detector.

## 1.2 Introduction of Conventional Scintillators and Crystal Growth Methods

### 1.2.1 Conventional Scintillator Single Crystals

Figure 1.2 shows the history of the development of scintillator crystals with the progress of crystal growth method. The development of scintillator single crystals has progressed along with that of crystal growth technology. In order to indicate excellent luminescence and scintillation performance (high light yield, great energy resolution, high transparency etc.), scintillator single crystals are required to be of high quality, and, as a result, progress in crystal growth technology is also highly recommended.

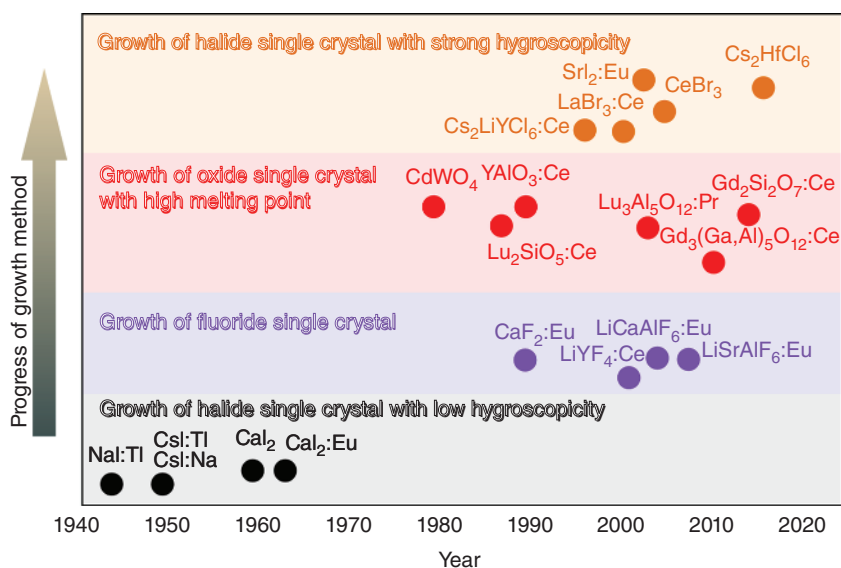


**Figure 1.2** History of the development of scintillator crystals with progress of growth method.

First, CsI:Tl and NaI:Tl single crystals were developed as the most familiar and inexpensive scintillator single crystals [1, 2]. They are widely used in application devices because these large bulk single crystals can easily be grown by the conventional melt-growth method and they have relatively low hygroscopicity.

After that, various oxide scintillator single crystals have been developed along with the establishment of crystal growth methods using precious metal crucibles such as iridium (Ir) and platinum (Pt) for oxide single crystals with a high melting point near 2000 °C. Among them, typical oxide scintillator single crystals are the garnet-type  $\text{Y}_3\text{Al}_5\text{O}_{12}:\text{Ce}$  and  $\text{Lu}_3\text{Al}_5\text{O}_{12}:\text{Pr}$ , perovskite-type  $\text{YAlO}_3:\text{Ce}$  and  $\text{LuAlO}_3:\text{Ce}$ , and silicate-type  $\text{Lu}_2\text{SiO}_5:\text{Ce}$ ,  $(\text{Lu},\text{Y})_2\text{SiO}_5:\text{Ce}$ , and  $\text{Gd}_2\text{SiO}_5:\text{Ce}$  [3–9]. In addition, as a high-density and effective atomic number scintillator,  $\text{Bi}_4\text{Ge}_3\text{O}_{12}$ ,  $\text{CdWO}_4$  and  $\text{PbWO}_4$  have been developed for detection of high-energy radiation [10–12].

Around the year 2000, global attention was focused on the high scintillation properties (high light yield and great energy resolution) of halide single crystals. However, many of the halide materials have strong hygroscopicity, and it was difficult to grow high-quality single crystals. Therefore, various techniques for growing single crystals of halide materials with strong hygroscopicity have been developed since then, and the development of halide scintillator single crystals has largely progressed. As a result, halides scintillator single crystals were first developed, centering on binary compounds such as  $\text{LaBr}_3:\text{Ce}$ ,  $\text{CeBr}_3$ , and  $\text{SrI}_2:\text{Eu}$  with high light yield and great energy resolution [13–15]. After that, the material research expanded to complex compounds of halide materials such as  $\text{Cs}_2\text{HfCl}_6$  and  $\text{Cs}_2\text{LiLaBr}_6:\text{Ce}$  [16, 17]. In recent years, high-performance chloride scintillator single crystals with relatively low hygroscopicity compared to bromide and iodide scintillator single crystals have been refocused, and they have been actively studied [18, 19].

## 1.2.2 Feature of Single Crystal

### 1.2.2.1 Characteristics of Single Crystal

Single crystals consist of a single grain, and they have a lot of special characteristics derived from the structure. Schematic diagrams of single crystal and polycrystalline are shown in Figure 1.3. There is no grain boundary in the single crystal and no grain boundary enables high transparency even in crystal systems with refractive index anisotropy. This high transmittance enables its use in optical applications. In the materials with cubic structure without the refractive index anisotropy, various transparent ceramics with high transparency have been developed by eliminating voids in grains and grain boundaries. However, the transmittance of the transparent ceramics decreases as the thickness increases, while the transmittance of single crystals without voids and cracks doesn't change even if the thickness is changed. Furthermore, the transmittance of transparent ceramics decreases even if voids are eliminated in a material system with refractive index anisotropy. Therefore, some single crystals have been applied for optical devices such as laser, lens, wavelength conversion element, and nonlinear materials and scintillators.

In addition, a single crystal has only “one” crystal orientation because it is composed of a single grain. As a result, it is possible to develop devices using

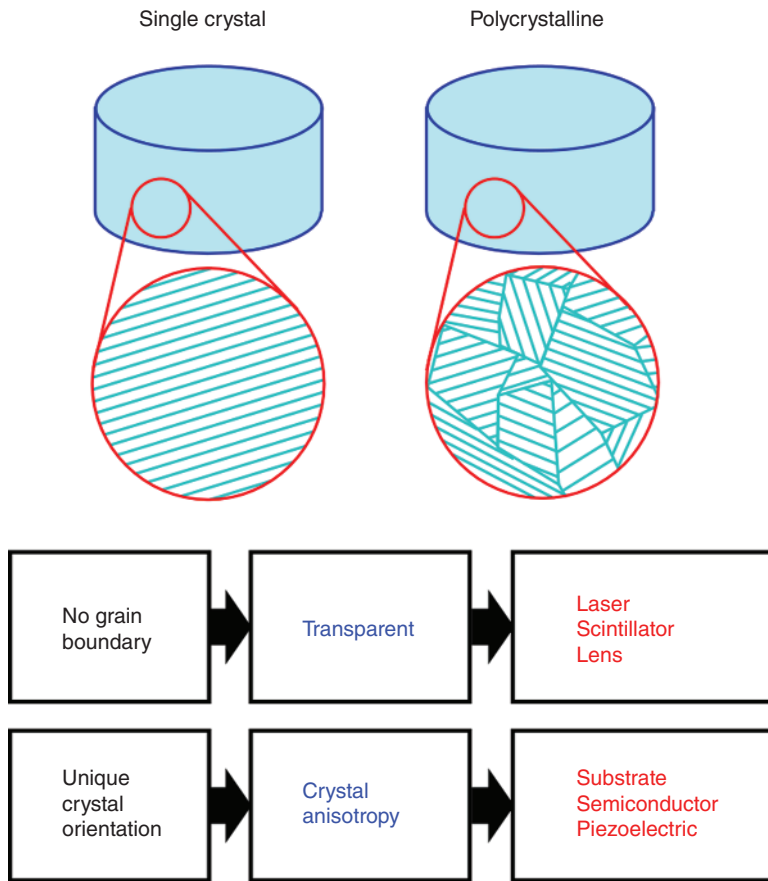


**Figure 1.3** Schematic diagrams of single crystal and polycrystalline.

crystal anisotropy of materials, and it enables the use of crystal orientation that indicates the best properties of functional materials. Therefore, single crystals are used in various fields using crystal anisotropy such as semiconductors, substrates, piezoelectric elements, and magnetic and electronic materials. For example, in the piezoelectric and semiconductor crystals, the crystal orientation that maximizes their piezoelectric and electrical properties is used, respectively. In the substrate crystal, the crystal orientation with the lattice constant that best matches that of the deposition material is chosen.

#### 1.2.2.2 Growth Methods of Single Crystal

Single crystals of materials with the congruent composition can be grown from the melts by the unidirectional solidification under a temperature gradient, and it is the “melt-growth method.” Various melt-growth methods such as Czochralski (Cz), Bridgman–Stockbarger (BS), and Floating Zone (FZ) have been developed for researches and commercial uses, and of course they have been also used for development of scintillator single crystals. Especially, Cz and BS methods can grow



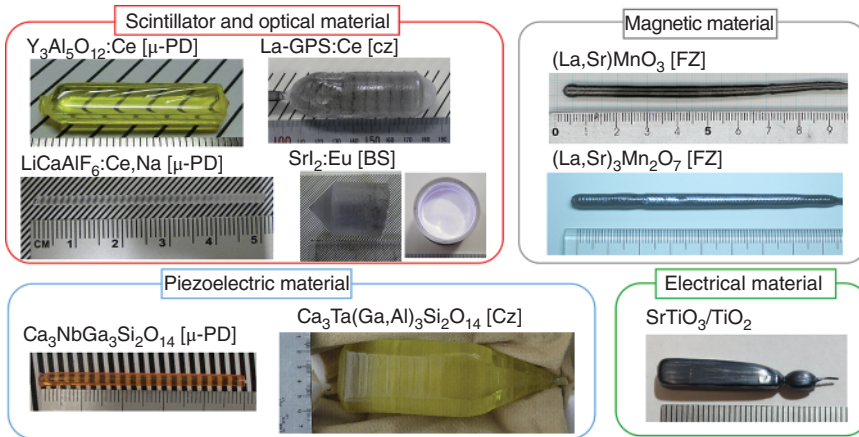


**Figure 1.4** Single crystals grown by Cz, BS, FZ, and  $\mu$ -PD methods.

a large bulk single crystal, and they have achieved mass production of the functional single crystals. On the other hand, micro-pulling-down ( $\mu$ -PD) and laser heating pedestal growth (LHPG) methods have been recently used for material research of functional single crystals because of the faster growth rate than conventional melt-growth methods such as Cz and BS methods. As a result, various novel single crystals have been developed by the  $\mu$ -PD and LHPG methods. Figure 1.4 displays single crystals of sapphire, scintillator, piezoelectric material, laser material, and magnetic and electrical materials grown by Cz, BS, FZ, and  $\mu$ -PD methods.

Many scintillator single crystals represented by  $\text{NaI:Tl}$ ,  $\text{CsI:Tl}$ , and  $\text{Lu}_2\text{SiO}_5:\text{Ce}$  have been developed by the melt-growth methods, and the developments and applications of radiation detectors equipped with the scintillator single crystals have progressed. On the other hand, novel melt-growth methods have been developed to perform material research in areas that have not been explored so far for various reasons recently. As a result, the development of various novel scintillator single crystals is proceeding with newly developed and modified melt-growth methods.

### 1.2.2.3 Segregation

Some scintillator single crystals include dopant element as an emission center such as  $\text{NaI:Tl}$ ,  $\text{CsI:Tl}$ , and  $\text{Lu}_2\text{SiO}_5:\text{Ce}$ , and the solid solution is used for improvements of scintillation properties by controls of the band structure and the crystal field around the emission center such as  $(\text{Lu,Y})_2\text{SiO}_5:\text{Ce}$  and  $\text{Gd}_3(\text{Ga,Al})_5\text{O}_{12}:\text{Ce}$ . In addition, starting materials contain small amounts of impurities even if they are of high purity, and the amount and distribution of impurities in the scintillator single crystals may affect the scintillation properties. In the crystal growth from the melt of the solid-solution system, chemical composition of the single crystal becomes non-uniform or impurity phases precipitate. That is, “segregation.”

Figure 1.5 shows the phase diagram of a binary complete solid-solution system, AO–BO. According to the phase diagram, 50 mol%AO liquid phase ( $C_1$ ) and 20 mol%BO solid phase coexist in equilibrium at a temperature  $T$ . “Distribution

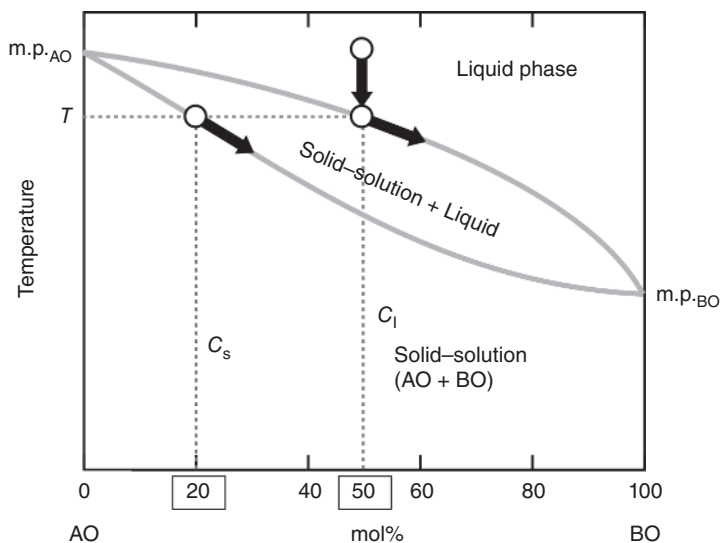


**Figure 1.5** Phase diagram of a binary complete solid-solution system, AO-BO.

coefficient,  $k$ ” is used as a factor indicating the degree of difference between the compositions at solid and liquid phases. “Equilibrium distribution coefficient,  $k_{eq}$ ” is the composition ratio of the liquid and solid phases that can be read from the phase diagram, and it is represented by the following equation.

$$k_{eq} = \frac{C_s}{C_l}$$

In the case of  $k_{eq} < 1$ , the solute concentration in the solid phase becomes lower than that in the liquid phase. On the other hand, in the case of  $k_{eq} > 1$ , the solute concentration in the solid phase becomes higher than that in the liquid phase. And at  $k_{eq} = 1$ , the solute concentration in the solid and liquid phases is matched. In the AO-BO system with  $k_{eq} < 1$ , when the starting material of 50 mol%BO ( $C_l$ ) is melted and the liquid phase is cooled, the crystal of 20 mol%BO ( $C_s$ ) is precipitated at the temperature  $T$ , and the concentration of BO in the liquid phase increases above 50 mol%BO. As it cools further, the composition of the liquid and crystal phases changes to the BO excess side. As a result, the concentration of BO in the precipitated crystal increases continuously from 20 mol%BO.

The distribution of solute concentration in the crystal varies depending on the growth method. Cz and BS methods crystallize a starting material from one side after melting the entire it, and their growth methods are called “normal freezing method.” On the other hand, the FZ method crystallizes a starting material by melting part of a starting material and moving the melt relatively while supplying a starting material, and it is called “zone melting method.” Verneuil method performs starting material supply and crystallization at the same time, and it can be regarded as a kind of zone melting method. In the normal freezing and zone melting methods, the solute concentration in the crystal when crystallized by moving the sample or the heater is

expressed by the following equations [20]:

$$\text{Normal freezing method: } \frac{C}{C_0} = k(1 - g)^{k-1}$$

$$\text{Zone melting method: } \frac{C}{C_0} = 1 - (1 - k)e^{-k \frac{x}{l}}$$

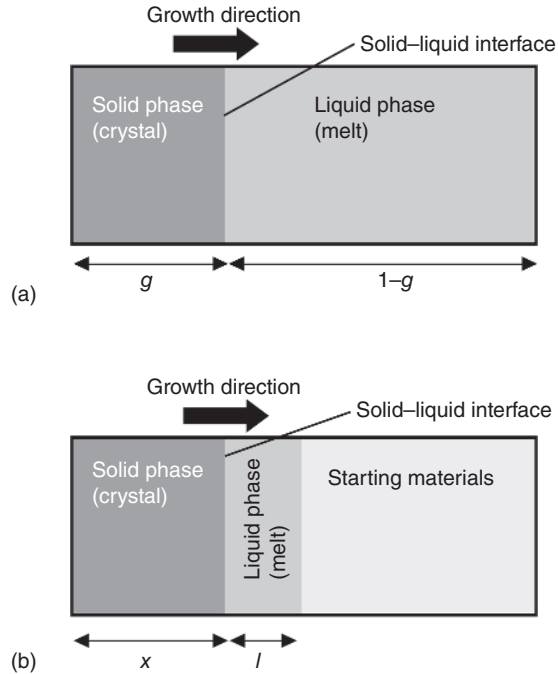
where  $C$  is the solute concentration in the crystal,  $C_0$  the solute concentration in the starting material,  $k$  the distribution coefficient,  $g$  the segregation for all starting materials,  $x$  the distance from initial crystallization, and  $l$  the length of melting zone. As shown in Figure 1.6a, in the normal freezing process, the relative concentration  $C/C_0$  changes continuously as the crystal growth progresses when  $k$  is not 1. On the other hand, in the zone melting process (Figure 1.6b), the solution concentration in the crystal approaches the concentration of starting materials as the crystal growth progresses.

When segregation occurs during the melt growth, supercooling may occur due to the concentration gradient of the melt around the solid–liquid interface. Figure 1.7 shows the schematic diagram of super cooling and cellular growth. At equilibrium state, the diffusion of atoms and ions in solid and liquid phases is extremely fast. Therefore, the solute concentration in the solid phase,  $C_s$ , is represented by

$$C_s = k_{eq} C_l$$

according to the phase diagram under the assumption of phase equilibrium. However, the diffusion of atoms and ions in the liquid phase is slow in actual crystal growth. Under this condition, the solid phase with a lower solute concentration than

**Figure 1.6** Schematic diagrams of (a) normal freezing and (b) zone melting processes.



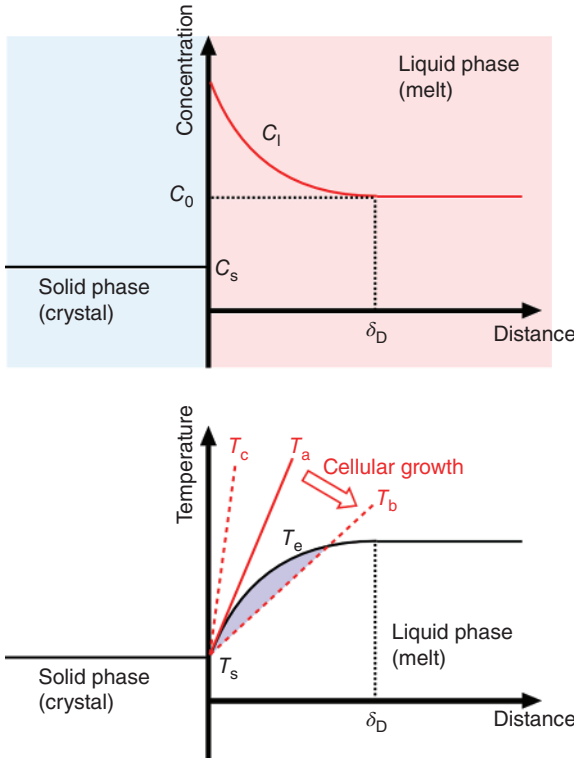


**Figure 1.7** Schematic diagrams of super cooling and cellular growth.

the liquid phase precipitates, and the concentration gradient due to diffusion occurs without sufficient agitation. The area is called “diffusion layer.” The solute concentration near the solid–liquid interface  $C_s'$ , becomes  $C_s' = k_{eq} C_1'$ , and it is greater than the solute concentration in equilibrium state  $C_s$ . At this time, the apparent distribution coefficient (effective distribution coefficient),  $k_{eff}$ , becomes  $k_{eff} = C_s' / C_1$ . The relationship between the effective distribution coefficient  $k_{eff}$  and equilibrium distribution coefficient  $k_{eq}$  can be expressed by the following formula [21].

$$k_{eff} = \frac{k_{eq}}{k_{eq} + (1 - k_{eq}) \exp\left(-\frac{v\delta}{D}\right)}$$

According to the formula, the effective distribution coefficient  $k_{eff}$  depends on the growth speed  $v$ , thickness of diffusion layer  $\delta$ , and diffusion coefficient  $D$ . The faster the growth speed, the closer  $k_{eff}$  is to 1.

In the diffusion layer, the solute concentration in the liquid phase decreases with increasing distance from the solid–liquid interface, resulting in an increase of the liquidus temperature. If the actual temperature gradient at the solid–liquid interface is greater than the gradient of the liquidus temperature, the region of the diffusion layer is in the liquid state. On the other hand, if the actual temperature gradient at the solid–liquid interface is less than the gradient of the liquidus temperature, supercooling occurs because the actual temperature is lower than the liquidus temperature.

Such a supercooling is called “compositional supercooling,” and the growth interface becomes unstable, making it easier for cellular growth to occur. Cellular growth is often confirmed in the growth of actual scintillator single crystals. For example, in a scintillator containing a dopant with a small  $k_{\text{eff}}$ , cellular growth occurs due to the compositional supercooling when the dopant concentration is relatively high.

#### 1.2.2.4 Crystal Structure

Simple lattices are classified into 14 types of Bravais lattices as shown in Figure 1.8. Cubic structure has the same lattice constant on all axes,  $a$ ,  $b$ , and  $c$ , and all axes are orthogonal. As a result, many transparent ceramics with the cubic structure have been developed because the refractive index is the same in all directions [22–24]. Even during the crystal growth of single crystal with the cubic structure, cracks in the grown single crystal are less likely to occur because there is no anisotropy of lattice

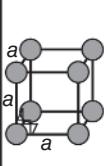
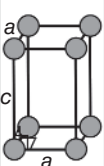
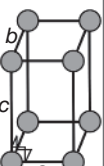
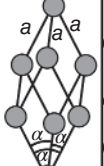
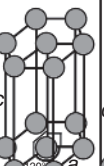
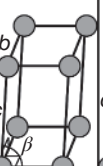
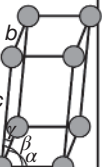
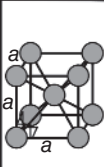
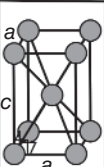
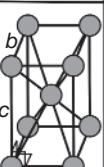
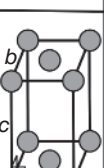
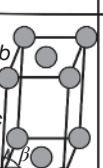
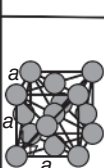
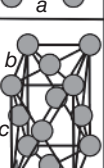
	Cubic	Tetragonal	Ortho rhombic	Rhomb ohedral (trigonal)	Hexagonal	Mono clinic	Triclinic
	$a = b = c$ $\alpha = \beta = \gamma = 90^\circ$	$a = b \neq c$ $\alpha = \beta = \gamma = 90^\circ$	$a \neq b \neq c$ $\alpha = \beta = \gamma = 90^\circ$	$a = b = c$ $\alpha = \beta = \gamma < 120^\circ$ ( $\neq 90^\circ$ )	$a = b \neq c$ $\alpha = \beta = 90^\circ$ $\gamma = 120^\circ$	$a \neq b \neq c$ $\alpha = \gamma = 90^\circ$ $\beta \neq 90^\circ$	$a \neq b \neq c$ $\alpha \neq \beta \neq \gamma$
Primitive cell							
Body- centered cell							
Side- face- centered cell							
Face- centered cell							

Figure 1.8 Bravais lattices.

changes (extension and contraction) during the cooling process. Many garnet-type and perovskite-type scintillator single crystals with the cubic structure are being mass produced [25, 26].

Tetragonal is a cubic structure extended (contracted) in one direction, and it also has relatively high symmetry. Materials with the tetragonal structure may have plate-like crystal shape and consist of plate-shaped grains, and orientation may be exhibited by the plate-shaped grains. Orthorhombic is a tetragonal structure extended (contracted) in another direction, and all lattice constants are different. In the case of the orthorhombic material with large anisotropy, cracks are likely to occur during the crystal growth and cooling process due to the differences in linear expansion coefficient for each direction. Since the growth rate varies with orientation in the materials with the orthorhombic structure, the choice of growth direction can be an important factor in the case of crystal growth by unidirectional solidification. Although all angles between axes of rhombohedral (trigonal) and hexagonal are not  $90^\circ$ , the symmetry is relatively high, and their structures are suitable for growing single crystals. On the other hand, monoclinic and triclinic have low symmetry compared to other structures, and cracks are generally more likely to occur. Therefore, for materials with the structures with low symmetry such as orthorhombic, monoclinic, and triclinic, the selection of the growth direction is one of the most important factors to improve the crystal quality and decrease cracks during the crystal growth. In addition, it is necessary to select a slower growth rate for materials with the low symmetric structures.

#### 1.2.2.5 Crystallinity and Defects

Crystallinity is one of the important factors for evaluating the crystal quality of single crystals. All single crystals are not perfect single crystals and have various kinds of defects. Crystallinity is an indicator of how far from perfect the single crystal is, and improvement of the crystallinity results in higher quality of single crystals. Single crystals include various kinds of defects in the lattice structure, and the most common defects are Schottky and Frenkel defects. They are illustrated in Figure 1.9. The defects are generated from the entropy effect of heat and are called “intrinsic defect.” In the case of the Schottky defect, both defects of cation and anion are generated simultaneously to maintain electrical neutrality in the crystal as illustrated in Figure 1.9a. When an ion is displaced from the regular position to the interstitial position, a defect pair of the defect at the regular position and the interstitial ion is formed, which is called “Frenkel defect” (Figure 1.9b). To generate the interstitial ion in the lattice, the ionic radius is important factor, and it generally occurs in the case of cations with a relatively small ionic radius.

When cations with the same valence and similar ionic radii are included in chemical compositions such as the garnet-type structure, the anti-site defect occurs owing to the two cations exchanging positions (Figure 1.9c) [27]. The anti-site defect becomes a factor in deteriorating the luminescence properties of scintillator single crystals by creating new energy levels in the band structure [28], and there are some reports regarding the mechanism and countermeasures of the anti-site defects.

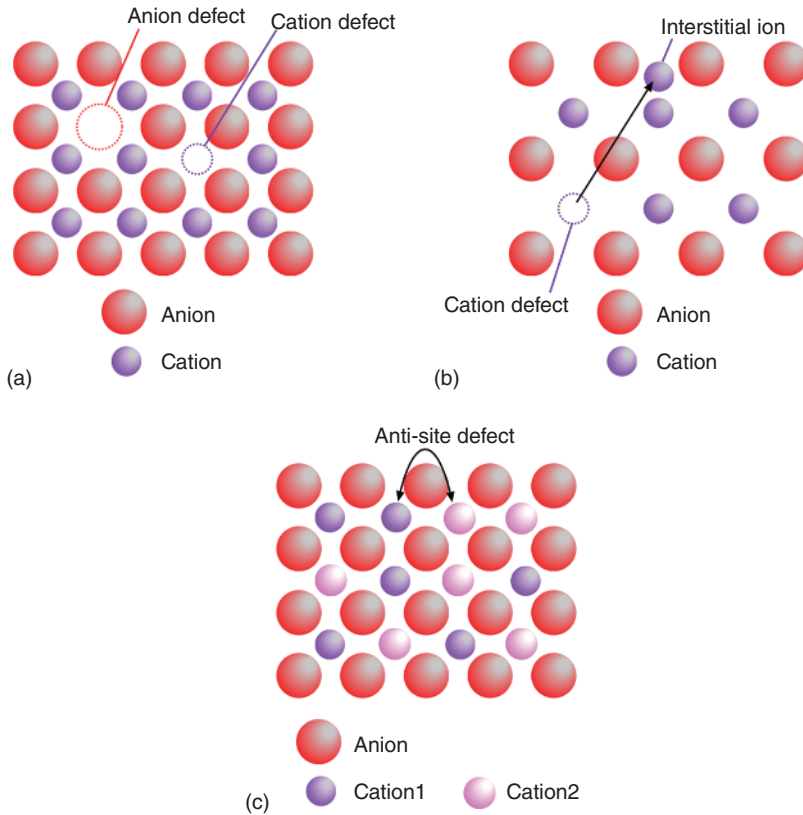


**Figure 1.9** (a) Schottky, (b) Frenkel, and (c) anti-site defects.

On the other hand, there are “extrinsic defects” generated from the external factors such as doping of ion with different valence and control of atmosphere during the crystal growth. In the material with dopant ion (cation) with difference valence, anion defects were generated to achieve the electrical neutrality condition around the dopant ion as illustrated in Figure 1.10a. Then, the material including a transition element may become a nonstoichiometric composition depending on the growth and annealing conditions. For example,  $\text{TiO}_2$  is composed of  $\text{Ti}^{4+}$  ion (cation) and  $\text{O}^{2-}$  ion (anion), and Ti is a transition-metal element. Therefore, when  $\text{TiO}_2$  single crystal is grown under reduction atmosphere, part of  $\text{Ti}^{4+}$  ion becomes  $\text{Ti}^{3+}$  ion and defects of oxygen site are generated (Figure 1.10b). As a result, the  $\text{TiO}_{2-\delta}$  single crystal grown under reduction atmosphere shows black color originating from the oxygen defect [29].

Crystallinity can be evaluated by the X-ray diffraction measurements. X-ray rocking curve (XRC) is the  $\omega$  scan on each diffraction peak using the X-ray diffractometer with four axes ( $2\theta$ ,  $\chi$ ,  $\phi$ , and  $\omega$ ) (Figure 1.11a). The broadening and splitting of the XRC peak indicate the degree of the crystallinity for the single crystal. The sharper the XRC peak, the higher the crystallinity. In addition, peak splitting and appearance of satellite peaks suggest the presence of polycrystallization and mosaic structure,

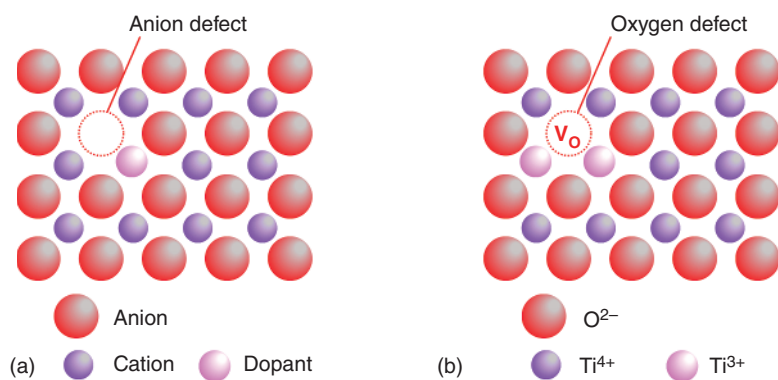


**Figure 1.10** (a) Doping of ion with different valence and (b) oxygen nonstoichiometry of  $TiO_{2-\delta}$ .

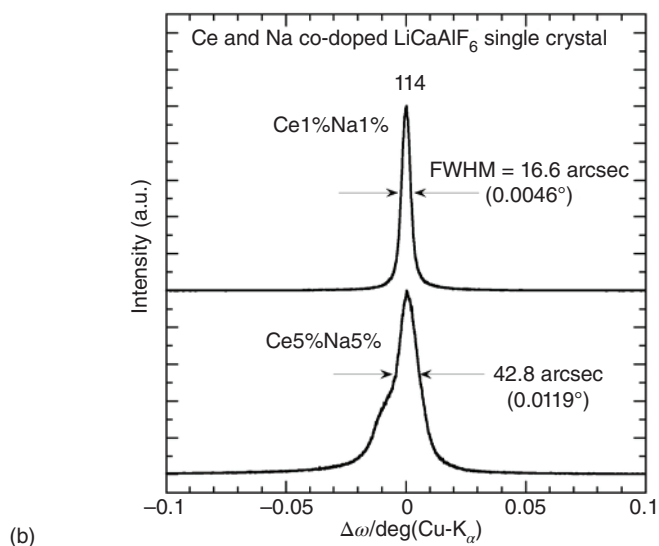
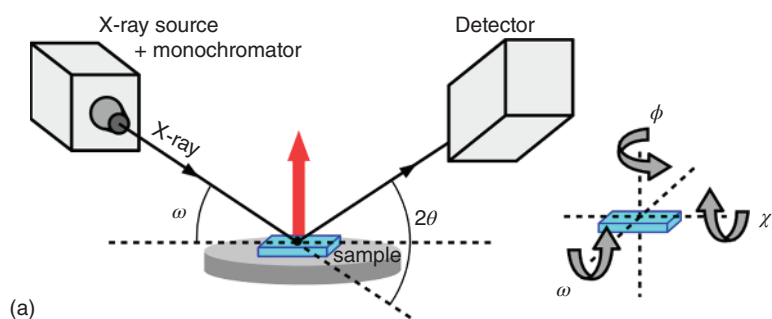


**Figure 1.11** (a) Schematic diagram of XRC measurement and the X-ray diffractometer with 4 axes. (b) XRC of  $LiCaAlF_6:Ce,Na$  single crystals [30].





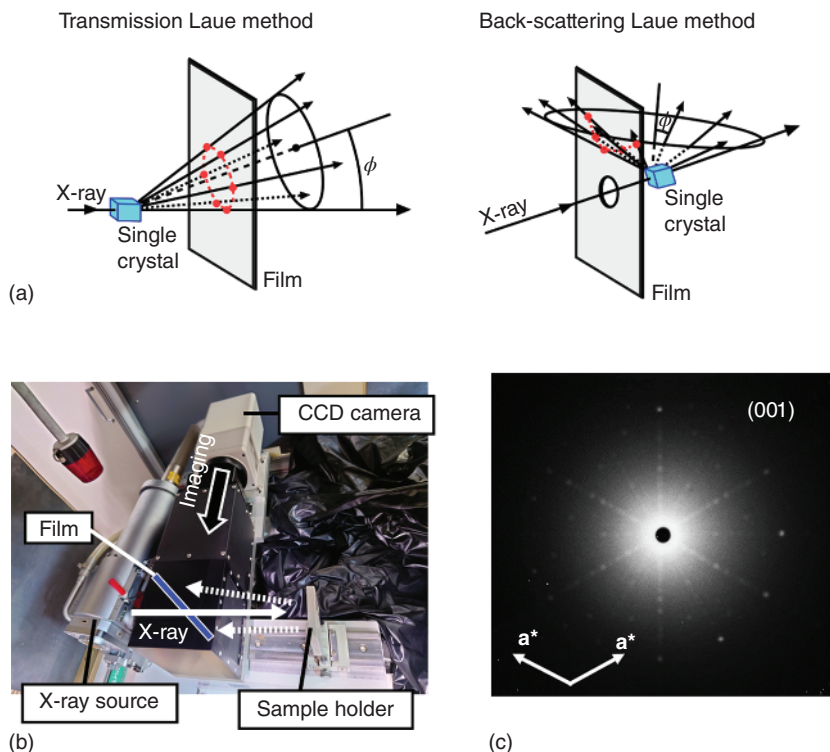


**Figure 1.13** (a) Schematic diagrams of Laue camera, (b) Laue camera device using CCD camera, and (c) back-scattering Laue image of trigonal structure.

orientation of crystal grains. Although the observation magnification is lower than that of EBSD and the orientation cannot be determined, the orientation alignment can be easily confirmed by the polarizing microscope using the cross Nicol method. It is possible to easily observe the presence and distribution of distortions in a bulk single crystal.

### 1.2.3 Crystal Growth Methods for Scintillator Single Crystals

#### 1.2.3.1 Czochralski Method

**Principle of Cz Method** Czochralski (Cz) method was developed by Jan Czochralski (1885–1953, Poland) [31]. When he put a pen in a crucible where the metal was melted by mistake for ink, he came up with the Cz method because the thin metal solidified by the capillary tube of the pen tip was a single crystal. The Cz method is one of the melt-growth methods with most established principle and equipment, and it can grow a large bulk single crystal with high crystallinity from the melt. Therefore, the Cz method has been used for mass production of various conventional single crystals including scintillators, and growth of various scintillator single crystals such as  $\text{Lu}_2\text{SiO}_5$  and garnet-type oxides ( $\text{Lu}_3\text{Al}_5\text{O}_{12}$  and  $\text{Y}_3\text{Al}_5\text{O}_{12}$ ) has been performed by the Cz method [32–34].

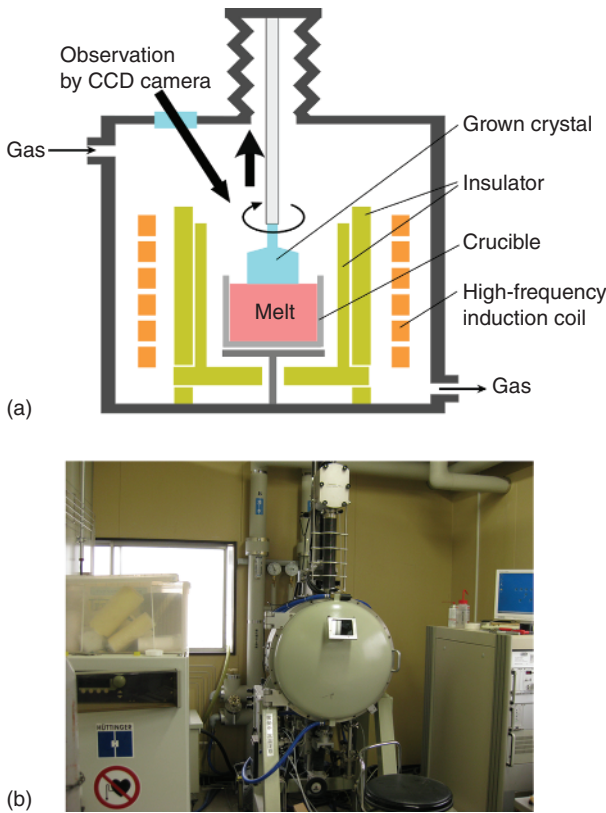


**Figure 1.14** (a) Schematic diagram and (b) actual furnace (high-frequency induction heating type) of Cz method.

There are two types of the Cz method, one is resistance heating-type Cz method and another is high-frequency induction heating-type Cz method. Both types of the Cz method use a crucible with twice larger diameter than the grown single crystal, and the bulk single crystal is grown from the melt in the center part of the crucible using a seed crystal. The schematic diagram and actual furnace of the high-frequency induction heating-type Cz method is shown in Figure 1.14.

**Crucible for Cz Method** A single crystal can be grown without restrictions from the crucible by the Cz method, and the grown single crystal has a freely grown surface with high crystallinity (Figure 1.14a). Therefore, a single crystal with an outer shape derived from the crystal structure can be obtained, and the shape is due to the crystal orientation dependence of the growth rate. Therefore, especially in the case of the Cz method, the crystal orientation of growth direction is important for obtaining the required bulk single crystal, and the crystal orientation of growth direction affects the growth rate and the frequency of crack and distortion occurrences in the grown single crystal.

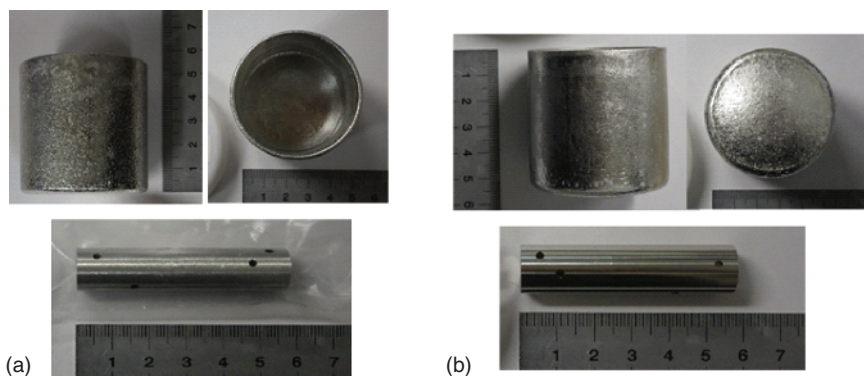


**Figure 1.15** (a) Ir crucible and seed holder for Cz method. (b) Pt-Rh crucible and reinforced Pt seed holder for Cz method.

Some oxide materials have high melting point and, currently, the high-frequency induction heating-type Cz method using a noble metal crucible such as iridium (Ir) or platinum (Pt) is mainstream (Figure 1.15) [35, 36]. The Ir crucible can be used up to  $\sim 2100^{\circ}\text{C}$ , while oxygen concentration in growth atmosphere is limited to approximately 2% due to the high oxidative reactivity at high temperature. The Ir crucible gradually becomes thinner by use under high temperature and high oxygen concentration, and eventually it will be necessary to recast the crucible. On the other hand, the Pt crucible can be used even under 100% oxygen because of the high oxidation resistance. In addition, molybdenum (Mo) and tungsten (W) crucibles are also used in some of the sapphire single crystal growth [37]. However, the Mo and W crucibles are more easily oxidized at high temperatures than the Ir crucible, and they are often used in a reducing atmosphere such as  $\text{Ar} + 2\text{--}3\%\text{H}_2$ . In the Cz method, the seed holder used directly above the crucible can also be made of the same metal as the crucible. Therefore, in the case of Ir crucible, the Ir seed holder is used. However, in the case of Pt or Pt alloy crucible, the reinforced Pt seed holder is sometimes used for crystal growth at high temperatures since the Pt seed holder is easily deformed at high temperature.

**Characteristics of Cz Method** The control of the solid–liquid interface shape in the Cz method is most important to grow a high-quality single crystal without internal distortions. The shape of the solid–liquid interface in the Cz method depends on various parameters such as viscosity and thermal conductivity of the melt, temperature conditions in a furnace, and the shape of crucible. In general, the convexity toward the melt side becomes smaller by increasing the rotation rate of the grown crystal (Figure 1.16) [38]. In the high-frequency induction heating-type Cz method, the crucible is heated by HF induction coil, and starting materials are heated indirectly. Therefore, convection from the periphery to the center of the melt in the crucible is generated and the convection is “natural convection.” On the other hand, when the grown crystal is rotated during the crystal growth, a convection different from the natural convection occurs by centrifugal force due to the rotation and the convection

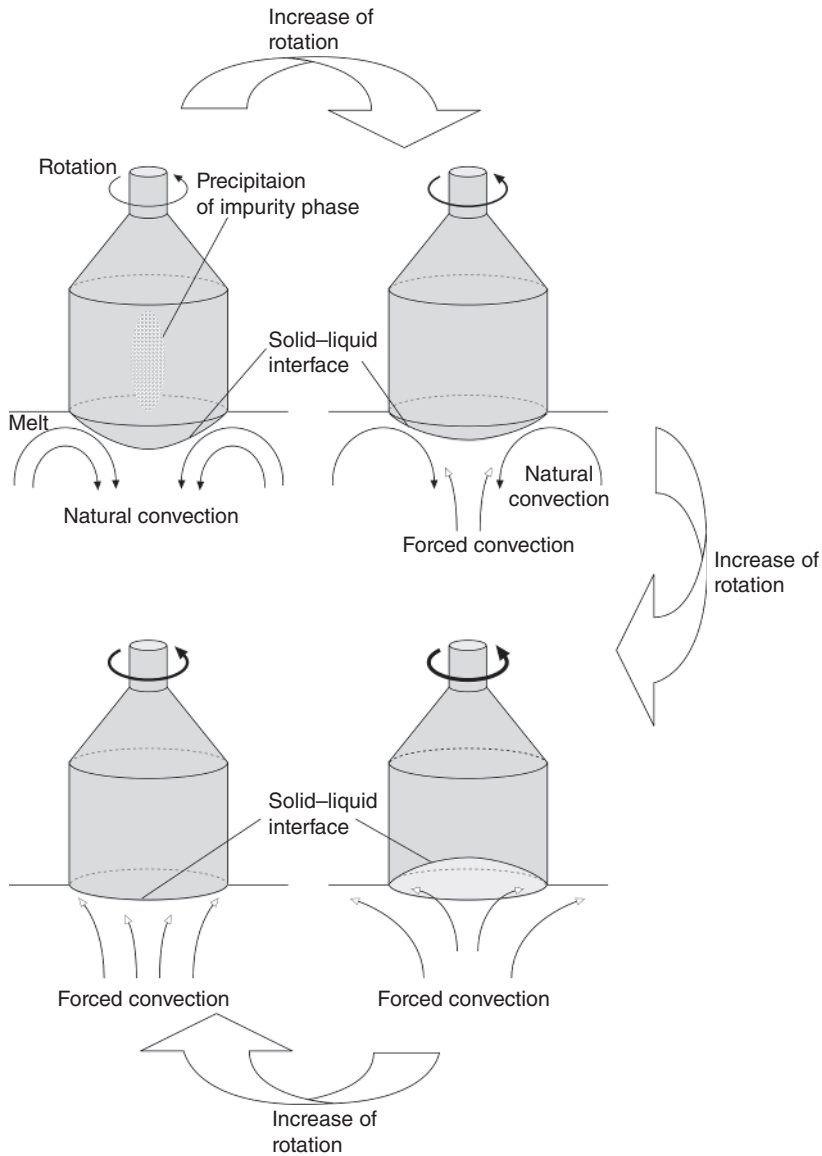


**Figure 1.16** Relationship between the solid-liquid interface shape and the rotation rate in the Cz method.

is “forced convection.” The shape of the solid-liquid interface during the crystal growth is changed by the balance between the natural and forced convections.

When natural convection with low rotation rate is dominant, the size of the convexity toward the melt (convex downward) at the solid-liquid interface increases, and abnormal segregation may occur at the center of the grown crystal due to the compositional supercooling. Abnormal segregation often occurs in scintillators and laser crystals with dopant. By increasing the rotation rate, the size of the convexity

toward the melt can be decreased, and abnormal segregation can be reduced. When the rotation rate is further increased, it becomes convex toward the crystal (convex upward) and interfacial disconnection may occur. Theoretically, the solid–liquid interface shape is derived using fluid parameters of “natural convection” and “forced convection” [39, 40]. The following relational expression holds between the crystal diameter:  $d$  and the rotational frequency:  $\omega$ .

$$d = \frac{(4g\beta\Delta TL^3\pi^{-2})^{1/4}}{\omega^{1/2}}$$

Here,  $g$  is the gravitational acceleration,  $\beta$  coefficient of thermal expansion of the melt,  $T$  temperature, and  $L$  diameter of the crucible. Theoretically, it means that the shape of the solid–liquid interface becomes flat under the growth condition that this expression holds. However, the expression depends not only on the physical properties of the melt, but also on parameters such as gas, heat flow, and radiation, and it doesn’t apply to all crystal growths. There are many things that depend on experience in the actual crystal growth, and it is necessary to carefully consider not only the rotation rate of the grown crystal but also various growth conditions.

Figure 1.17 shows bulk single crystals grown by the Cz method. Some single crystals have a characteristic shape, and the characteristic shape is derived from the difference in the growth rate of the crystal orientation. As described above, since the surface of the grown single crystal is free in the Cz method, a single crystal with a characteristic shape is grown, and the shape also depends on the growing crystal

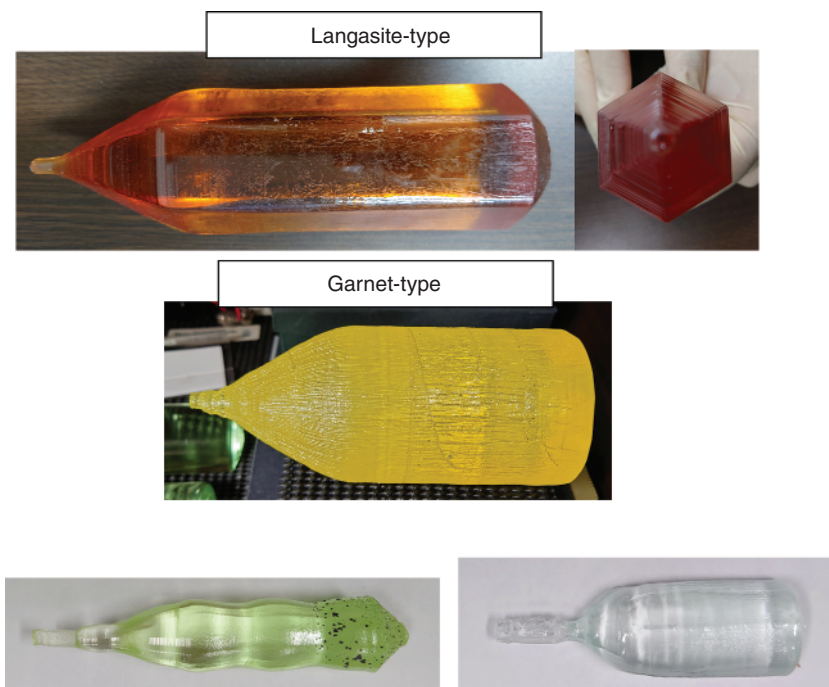


**Figure 1.17** Bulk single crystals grown by the Cz method.

orientation. The langasite-type single crystal with the trigonal system (hexagonal family) grown using a  $c$ -axis seed crystal shows a hexagonal shape.

**Segregation in Cz Method** In the Cz method, the partial mixing model with the no-mixing zone (diffusion layer) is used to analyze the actual segregation state of dopant in the host material and solid-solution material. As shown in Figure 1.18a, in the case of crystal growth of materials with the segregation coefficient far from 1,

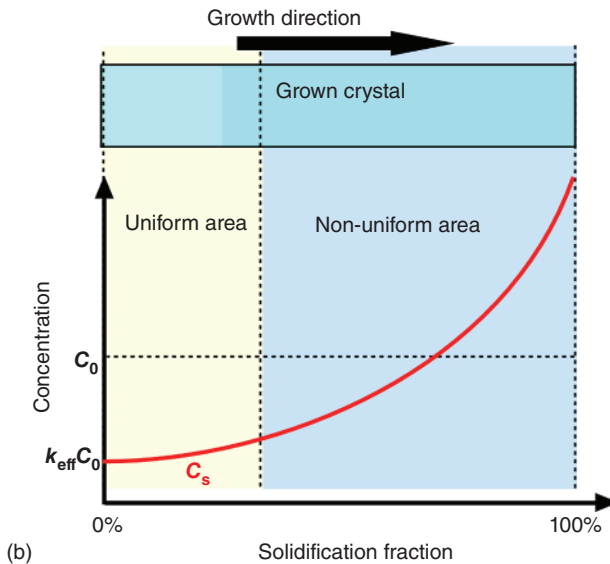
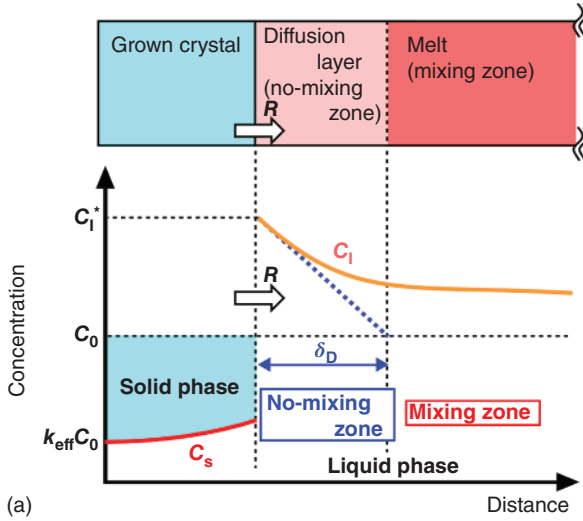


**Figure 1.18** Change of concentration during crystal growth in Cz method. (a) Uniform area at initial part and (b) all area at 100% solidification fraction.



the crystal growth should be finished in the region of uniform chemical composition at the initial part. The higher the solidification fraction (ratio of grown single crystal to total melt), the higher the productivity during the commercialization, but the value of the solidification fraction depends on the required performance of the crystal application. Particularly in the region of non-uniform area at the later part, a large change of concentration occurs (Figure 1.18b). Therefore, it is important to determine the target of the solidification fraction after analyzing the segregation state in the grown single crystal and clarifying the relationship between uniformity of chemical composition and properties.

When the diameter of the grown bulk single crystal is larger, the state of segregation in the radial direction may affect physical properties including optical and scintillation properties. If the crystal growth is performed at solid–liquid interface with a convex or concave shape, the dopant concentration and chemical composition of solid–solution material may differ between the center and the periphery areas in the radial direction. Therefore, it is also important to focus on the shape of the

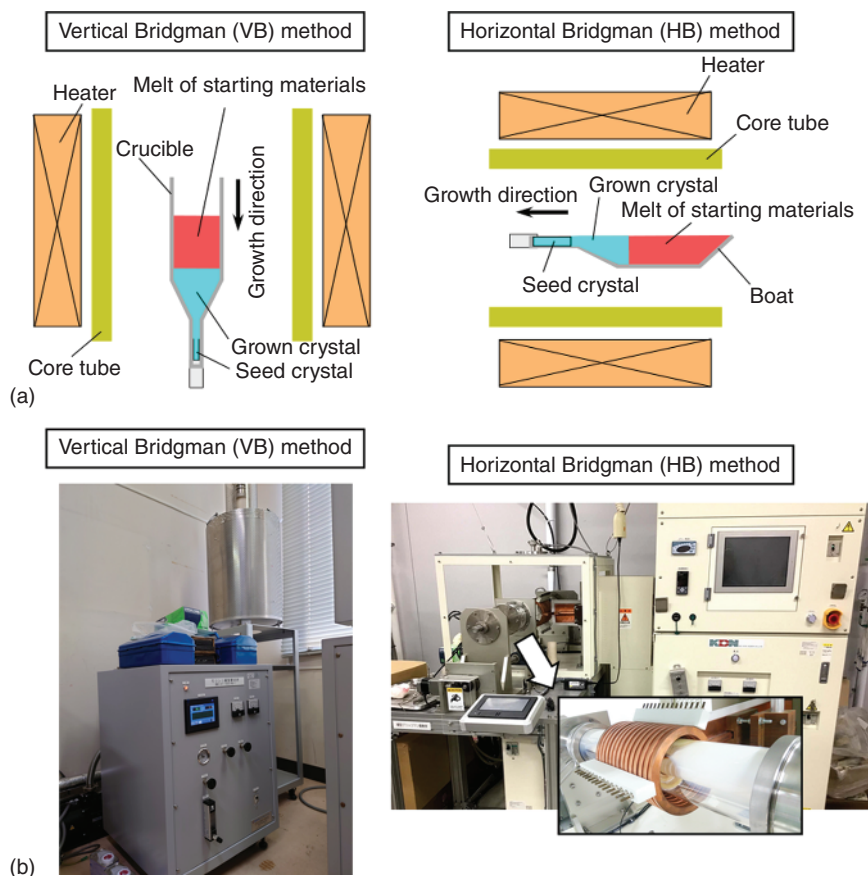


**Figure 1.19** (a) Schematic diagram and (b) actual furnace of VB with the resistive heating and HB method with the high-frequency heating.



solid–liquid interface during the crystal growth when the radial distribution of the dopant and chemical composition becomes a problem for the uniformity of physical properties. In general, the uniformity in the radial direction is improved by appropriately controlling the rotation rate of the grown single crystal and the temperature distribution in the furnace to flatten the solid–liquid interface.

### 1.2.3.2 Bridgman Method

**Principle of BS Method** Bridgman–Stockbarger (BS) method is one of well-known melt-growth methods, and a single crystal is grown in a crucible under temperature gradient [41, 42]. There are two types of BS method, vertical Bridgman (VB) and horizontal Bridgman (HB). The schematic diagrams of VB and HB methods, and actual furnaces are shown in Figure 1.19. In the furnace with temperature gradient, a crucible containing a melt of target material inside is moved vertically and horizontally in the VB and HB methods, respectively. Like the Cz method, the BS method has also been used for industrial production of various bulk single crystals.

**Principle of VGF Method** In addition, there is a vertical gradient freeze (VGF) method [43], and the principle of the VGF method is close to that of the VB method as illustrated in Figure 1.20. The VGF method also grows a single crystal inside the crucible in a furnace with a temperature gradient. However, unlike the VB method, the crucible doesn't move during the crystal growth in the VGF method, and the crystal growth is performed from the low-temperature side to the high-temperature side in the crucible by changing the temperature. In the VGF method, the starting materials in the crucible are melted by increasing the output of the heater or the HF power

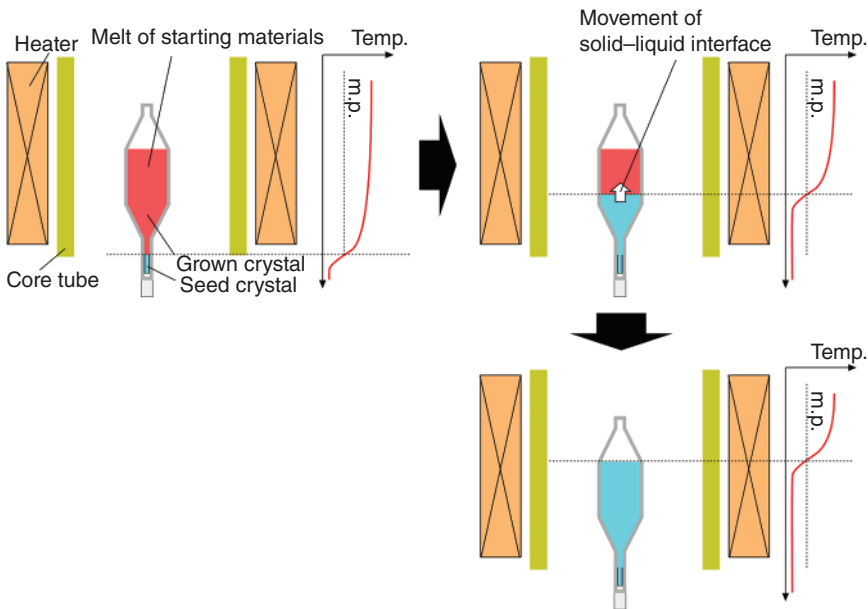


**Figure 1.20** Schematic diagram of the VGF method.

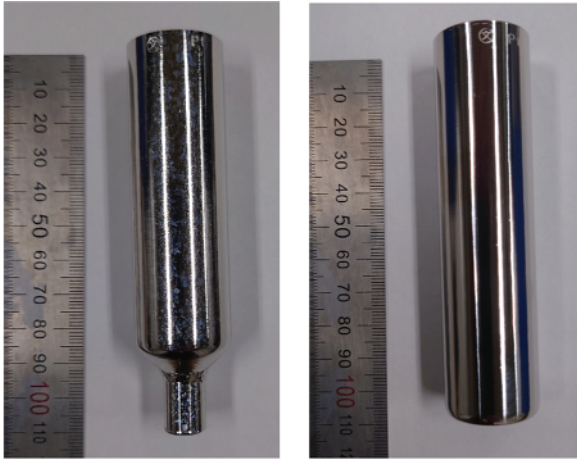
supply to raise the temperature in the furnace without changing the position of the crucible. After subsequent seeding, crystal growth is carried out in the crucible by gradually increasing the temperature. The VGF doesn't require an axis movement mechanism, and it is suitable for simplification and miniaturization of the furnace.

**Characteristics of BS and VGF Methods** At 1925, melt of metals in the mold (crucible) was crystallized for measurements of physical properties by Bridgman [42], and Stockbarger grew a LiF single crystal under large temperature gradient by the modified Bridgman's method [43]. Crucibles of various shapes are used, some of which have a simple body, a sharp bottom, and a thin tip. A seed crystal is set at the tip of the bottom of the crucible and a single crystal with high crystallinity can be obtained by growing from the seed crystal. In the VB method, the temperature inside the furnace is high in the upper part and low in the lower part. As a result, temperature gradient is formed in the furnace. By placing or pushing up the crucible containing starting materials at the upper part heated above melting point, the starting materials in the crucible melt. In addition, "seeding" is performed by melting the upper part of the seed crystal. Then, the crucible is pulled down and the melt is crystallized at a location below the melting point. The grown crystal is cooled slowly after all the melt is crystallized. The grown crystal has the same crystal orientation as the seed crystal. In the VB method, the growth rate is almost same as the pull-down rate of the crucible when the chemical composition of the melt doesn't change with solidification. Since the shape of the grown crystal is defined by the crucible, shape control mechanism is not required unlike the Cz method. In addition, cylindrical and prismatic shape single crystals can be grown by changing the shape of the crucible in the VB method.

The disadvantage of the VB and VGF methods is that it is not possible to directly observe the conditions inside the furnace and the crucible such as seeding, state of crystal and melt, and solid-liquid interface during the crystal growth. Seeding, which is one of the most important processes in the crystal growth, can't be observed and it often happens that the starting materials are not melted or the seed crystal is completely melted. As a result, growth of single crystal fails and polycrystallization occurs. In addition, the failure of the seeding process is unknown until the crystal is taken out because the crystal growth is not completed until the entire melt is solidified. On the other hand, the seed crystal and the melt are arranged horizontally in the HB method, and the solid-liquid interface and seeding during the crystal growth can be directly observed. However, a boat-shaped crucible must be used, and cylindrical single crystals can't be obtained.

**Crucible for BS and VGF Methods** VB and VGF methods are also a crystal growth method that uses a crucible like the Cz method, and it is important to select a material of the crucible (Figure 1.21). It affects the extraction of grown single crystals from the crucible, which was not necessary for the Cz method. As a major premise, it must be a material of the crucible that can be used stably at the melting point of the grown crystal without reaction with the melt. Furthermore, as a unique feature of the VB method that grows a single crystal in the crucible, it is important that the coefficient of thermal expansion of the crucible is smaller than that of the grown

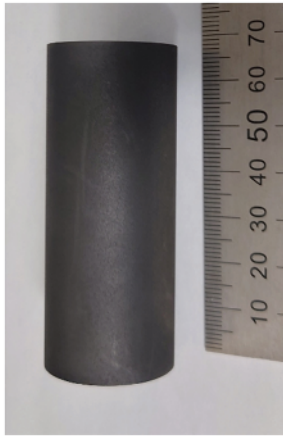
Platinum



Aluminium



Carbon

**Figure 1.21** Crucibles for the VB method.

crystal to obtain a high-quality single crystal with few cracks. Pt and Pt-Rh with relatively high melting point are often used for the crystal growth of oxides as a crucible material because of the strong oxidation resistance and excellent workability. Since the Pt and Rh metals are very expensive, a thin crucible is used for the crystal growth. And after the crystal growth, the crucible is stripped off from the grown crystal, and the crucible can be reused by refining and recasting. Ir, W, and Mo with higher melting point than Pt are sometimes used for crystal growth of materials with high melting point. However, they can't be used under oxidizing atmosphere. Carbon, SiC, and BN are also materials of the crucible in VB method, and they are also used under inert atmosphere. In addition, crystal growths of some materials excluding oxide are performed by the quartz glass,  $\text{ZrO}_2$ , and  $\alpha\text{-Al}_2\text{O}_3$  crucibles.

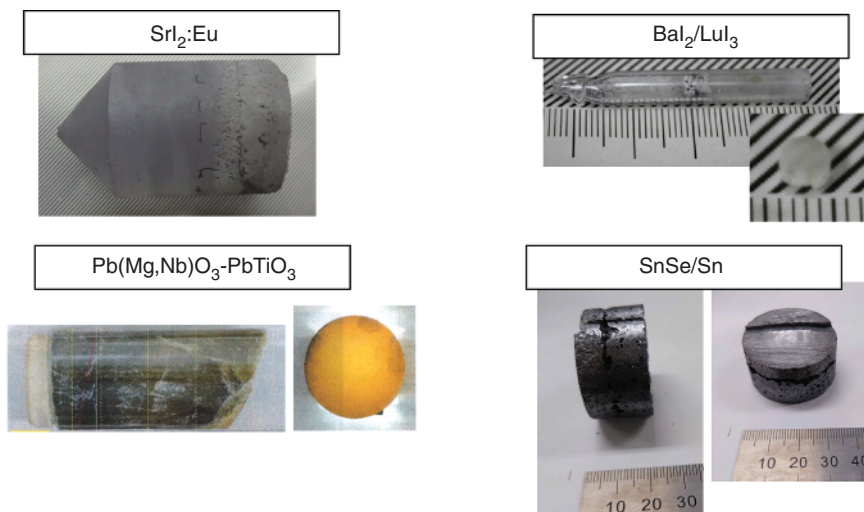


**Figure 1.22** Bulk single crystals grown by the BS method.

**Bulk Single Crystals Grown by BS Method** The VB method is also widely used in the growth of sapphire ( $\alpha\text{-Al}_2\text{O}_3$ ) bulk single crystals [44]. A sapphire single crystal with a melting point of  $2040^\circ\text{C}$  can be grown by the VB method using a W crucible in Ar atmosphere. The thermal expansion coefficient of the W is always smaller than that of sapphire in the temperature range from the melting point of room temperature. That is, the shrinkage of the sapphire single crystal is larger than that of the W crucible in the cooling process after the crystal growth. As a result, the grown bulk single crystal can be easily separated from the W crucible, and the bulk single crystal can be taken out without breaking the crucible by turning the crucible upside down. Therefore, in order to improve the quality of the grown single crystal in the VB method, the difference in thermal expansion coefficient between the single crystal and crucible is important (Figure 1.22).

### 1.2.3.3 Floating Zone Method

**Principle of FZ Method** FZ method is one of the melt-growth methods without a crucible. The FZ method forms a melt between the rod-shaped starting material and the grown single crystal by the local overheating and grows a single crystal by moving the melt [45–47]. Figure 1.23 shows the schematic diagram of infrared heating-type FZ method using halogen lamps. Unlike the Cz and BS methods, the FZ method doesn't use a crucible, and it holds the melt by the balance between the surface tension of the melt and gravity. Therefore, the crystal growth of the FZ method isn't restricted by the crucible, and there is no risk of contamination from the crucible. In addition, crystal growth under oxygen atmosphere and ultra-high temperature is possible because there is no risk of oxidation and melting of the crucible. Therefore, it is possible to grow single crystals of materials with high reactivity to the crucible and materials that easily volatilize in a reducing or inert atmosphere by the FZ method.

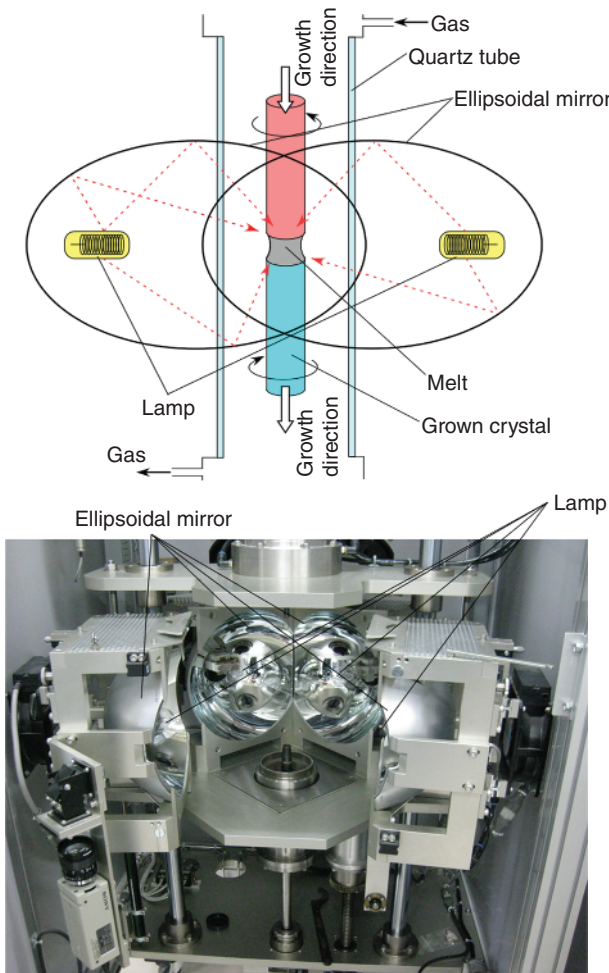


**Figure 1.23** The schematic diagram and actual furnace of infrared heating-type FZ method using halogen lamps.

**Characteristics of FZ Method** Then, in the FZ method, zone melting process is used for the crystal growth unlike the Cz and BS methods that grow a single crystal after melting all starting materials. The zone melting process melts a part of the starting materials and moves it to grow a single crystal. Therefore, in principle, it is possible to grow a single crystal with a uniform composition by making the composition of the melting zone an appropriate composition that is different from that of the starting material. There are some local heating types such as high-frequency heating and infrared heating using ellipsoidal mirrors in the FZ method. The high-frequency heating-type FZ method is used for the mass production of Si single crystal, and the crystal should have some conductivity in the method [48].

On the other hand, the infrared heating-type FZ method is more versatile because any material that absorbs infrared-rays can be heated and melted regardless of

whether it is conductive. In the infrared heating-type FZ method, centralized heating using halogen and xenon lamps with ellipsoidal mirrors [49–51], and laser heating [52] are available. In the case of the FZ method using the laser heating, it is difficult to melt materials that absorb very little emission light. The FZ method using the lamp heating can melt a wider range of materials because of the wider wavelength range of the light from the lamp. A halogen lamp can gradually heat the materials from room temperature, while it can't melt the material with high melting point than 2000 °C. On the other hand, a xenon lamp can grow a single crystal of the material with high melting point. However, it can't gradually heat the material from room temperature, and halogen lamps are more commonly used for the crystal growth by FZ method.

As I mentioned above, a rod-shaped starting material is needed in the FZ method, and it should be prepared in advance before crystal growth. The rod-shaped starting material is obtained by press molding the starting material powder with single phase into a cylindrical shape. There are some methods of the press molding such as the use of specific size molds and the hydrostatic pressure using a long rubber tube filled with the starting material powder. After the press molding, the molded rod is sintered at high temperature for the densification and the sintered rod is used for the crystal growth. In the case where the melt soaks into the starting material rod or bubbles are generated in the melt during the crystal growth, it is necessary to reconsider the conditions for producing the starting material rod such as sintering temperature and time, atmosphere, and pressure during press molding. In some cases, the starting material rod is melted and the melt is moved at several times to several tens of times faster speed than that in general crystal growth to prepare a molten-solidified rod, and it is used as a starting material rod.

In the infrared convergent floating zone (IR-FZ) method, local heating is realized by converging light from a single or multiple infrared light sources such as halogen and xenon lamps with ellipsoidal, parabolic, and spherical mirrors. In some cases, the focal point and light source are arranged vertically, but generally they are arranged in the same horizontal plane. There are types with one to six ellipsoidal mirrors, and the converged local heating in the circumferential direction becomes uniform as the number of light sources increases. On the other hand, there are some reports that the use of odd number of laser sources is more effective for homogenization of the local heating in the FZ method using the laser source [53].

In the growth process, the starting material rod is placed above the focal position and the lower end of the rod is melted first. After bringing the seed crystal placed below the focal position into contact with the melting zone of the starting material rod, the rod and the seed crystal are rotated in directions facing each other for stirring the melt. As a result, a molten zone is formed between the rod and the seed crystal, and crystallization occurs continuously at the interface on the bottom of the molten zone (between the melt and the grown crystal) by moving both the starting material rod and the seed crystal vertically downward. On the other hand, starting material is continuously supplied to the melt at the interface on the top of the molten zone (between the starting material rod and the melt). Like Cz and BS methods, the crystal orientation of the grown single crystal can be controlled by the seed crystal. It



is also possible to control the pressure of the growth atmosphere, and crystal growth under pressurized conditions up to  $\sim 1$  MPa has been reported [54]. During the crystal growth, it is necessary to continuously form a stable molten zone by optimizing various growth parameters such as the output of the light source, the feed and rotation rates of the starting material rod and the grown crystal, and the flow rate and pressure of the atmosphere gas for the stable crystal growth. The molten zone can be observed directly by a camera. However, only the melt surface is observable by the camera. Therefore, even if it seems to form an ideal molten zone, the inside of the molten zone may not be sufficiently melted, and the starting material and the grown crystal may come into contact with each other, resulting in dripping of the melt.

**Segregation of FZ Method** In the FZ method, no diffusion occurs in the starting material rod and the grown crystal while sufficient diffusion takes place in the molten zone. Therefore, assuming the unidirectional solidification that solidification occurs from the left end of the  $C_0$  concentration (dopant and impurity), the concentration of the first crystallized phase (initial crystal) is  $k_0 C_0$ . Here,  $k_0$  is the distribution coefficient. As a result, the concentration discharged from the grown crystal into the molten zone is

$$C_0 - k_0 C_0 = C_0(1 - k_0)$$

In other words, the concentration of the molten zone in contact with the solid–liquid interface increases, and as solidification proceeds, the  $C_1^*$  concentration (concentration of the molten zone) gradually increases. After the concentration reaches  $C_0/k_0$  at the molten zone, the crystal with  $C_0$  concentration is grown from the melt. As a result, only the molten zone migrates (travels) as crystal growth proceeds, and a single crystal with the same chemical composition as the starting material rod is grown. Since concentration increases again during the termination process, the concentration distribution in the grown crystal rod is as shown in Figure 1.24. As a result of the growth process, the segregation in a single crystal grown by the FZ method is as shown in Figure 1.25. Therefore, in the central part of the grown single crystal (constant stage), a single crystal with the desired uniform composition can be obtained.

**TS-FZ Method** As described above, the single crystal is grown by the molten zone held by the starting material rod and seed crystal (grown crystal) in the FZ method, so it is possible to use a solvent at the molten zone. First, the solvent placed on the seed crystal is melted, and then the starting material rod is adhered to the melted solvent. Crystal growth using the solvent is performed by relatively moving the melted solvent downward. The method is called “traveling solvent floating zone (TS-FZ) method,” and its schematic diagram is shown in Figure 1.26. The greatest feature of the TS-FZ method is that the use of the solvent enables crystal growth of the incongruent melting compound which cannot be grown by the Cz and BS methods [55, 56]. Furthermore, it is also possible to lower the melting point with a solvent. However, it is required to hold the molten zone more stably than the normal FZ method since the solvent can’t be added during the crystal growth.

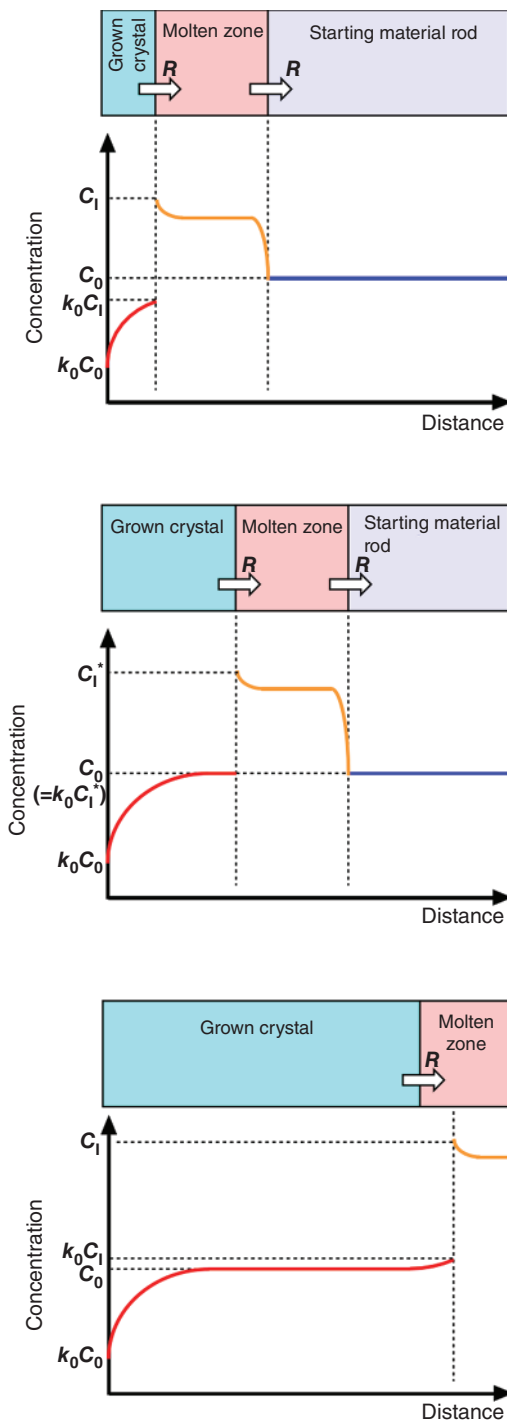


**Figure 1.24** Change of concentration during crystal growth in FZ method.



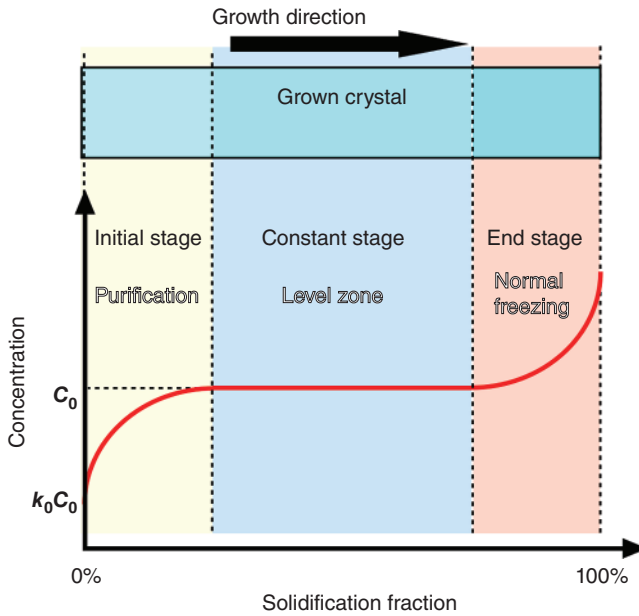


Figure 1.25 Concentration distribution in single crystal grown by FZ method.

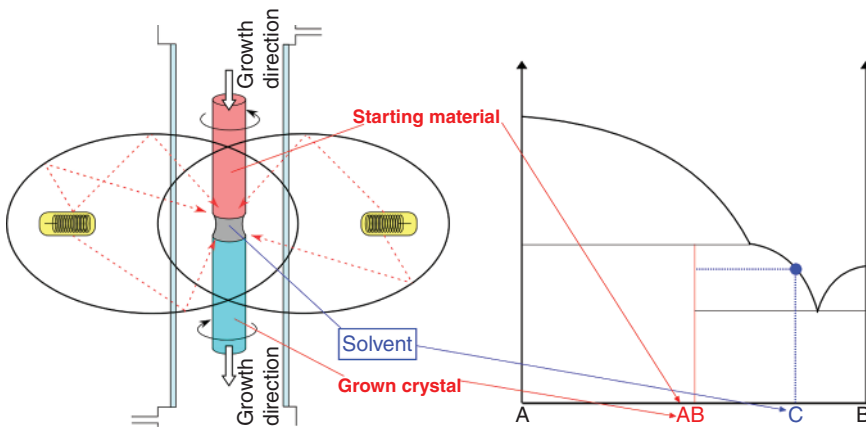


Figure 1.26 Schematic diagram of traveling solvent FZ (TSFZ) method.

#### 1.2.3.4 Micro-Pulling-Down Method

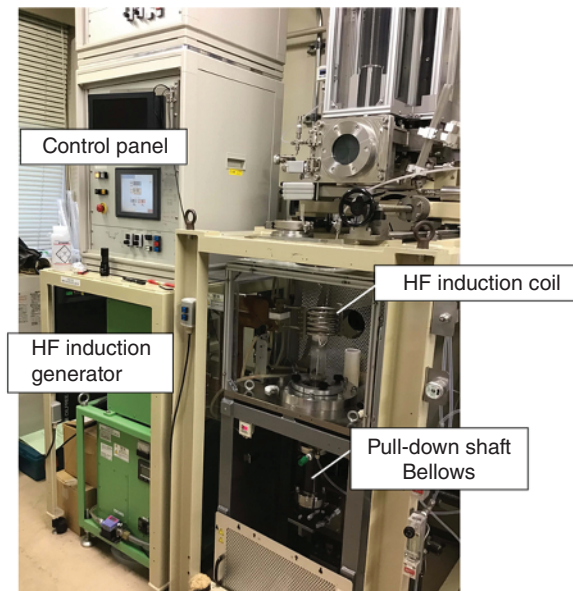
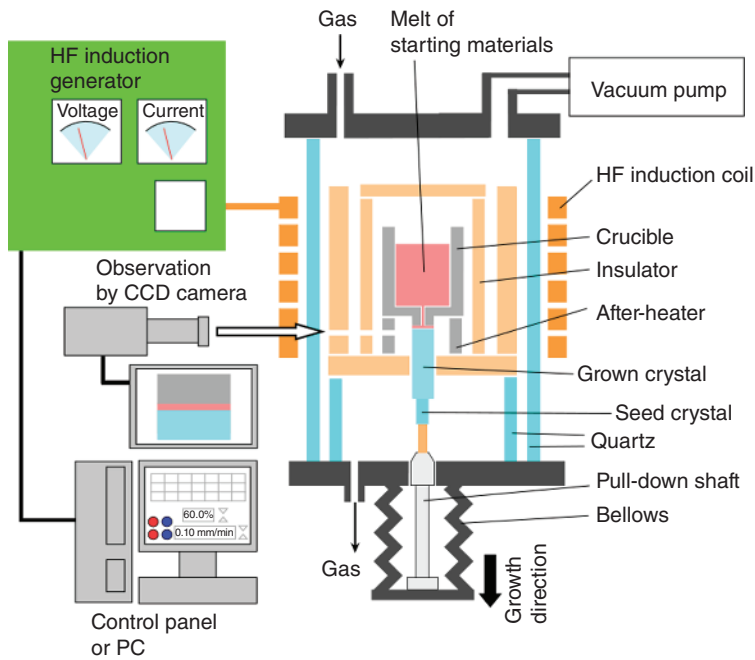
**Principle of  $\mu$ -PD Method** Micro-pulling-down ( $\mu$ -PD) method is one of the melt-growth methods using a crucible, and it is a crystal growth method developed in relatively recent years. The principle of the  $\mu$ -PD method had already been devised as the inverted Stepanov (IF) method, and the first paper of crystal growth by the  $\mu$ -PD method was published by Yoon et al. in 1994 [57]. At first, the  $\mu$ -PD method had been used for the crystal growth of semi-conductor single crystals [58, 59], and after that, research using the  $\mu$ -PD method had expanded to piezoelectric single

crystals represented by the langasite-type materials [60] and optical single crystals such as scintillators and laser materials [61]. In addition, the  $\mu$ -PD method can grow a shape-controlled single crystal using a specially designed crucible, and the shape-controlled growth technique has been developed for some functional single crystals [62, 63].

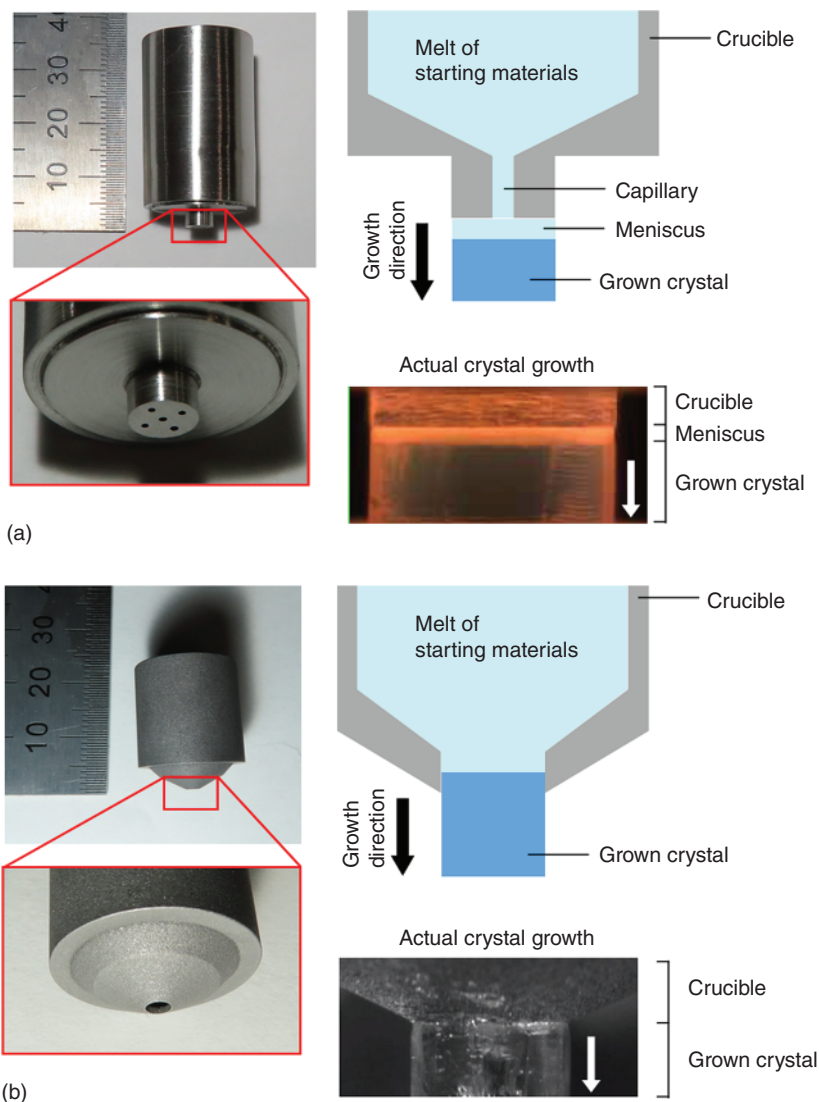
The  $\mu$ -PD method uses a crucible with a die on the bottom, and it grows a single crystal by pulling-down the melt in the crucible. The melt in the crucible reaches the bottom of the die through a hole (capillary) in the bottom of the crucible due to the capillarity, and the melt spreads wet on the bottom of the die. When the seed crystal is brought into contact with the melt on the bottom of the die (meniscus) and pulled down together, the melt was solidified (crystallized) under temperature gradient around the bottom of the die and the solid-liquid interface was generated. By continuous crystallization while controlling the thickness of the meniscus to be constant, a single crystal fiber can be fabricated.

Figure 1.27 shows a schematic diagram and photograph of the typical  $\mu$ -PD furnace for crystal growth of oxide material. There are two types of  $\mu$ -PD method, resistive heating type and high-frequency induction heating type like the Cz method. Here, the high-frequency induction heating type is explained because it is widely used at present. This furnace can be classified into the following six categories according to each function. The first is the “crystal growth section,” which is composed of starting materials, crucibles, and insulators. The starting materials and the crucible are heated by the “heating section,” consisting of a high-frequency power supply and a high-frequency induction coil. In the “pulling-down section,” a seed crystal attached to the pull-down shaft using a chuck is set, and the status of crystal growth can be observed in real time using the “observation section” consisting of a CCD camera and a monitor. In addition, there are the “atmosphere control section” consisting of a vacuum pump and a unit for introducing atmosphere gas for replacing gas in the furnace, and the “control section” that controls the high-frequency induction power supply, the pull-down shaft, and opens and closes valves.

**Crucibles of  $\mu$ -PD Method** In the high-frequency induction heating-type  $\mu$ -PD method, metal and carbon crucibles that can be heated by the induced current are used. However, when a metallic starting material is used, it is possible to heat the starting material by directly passing an induced current and, in that case, a ceramic crucible can also be used. It is necessary to select a material for the crucible that does not react with the melt of starting materials, and a precious metal crucible is generally used for growing an oxide single crystal. Ir and Pt crucibles that can be used at high temperatures are mainly used. However, rhenium (Re), molybdenum (Mo), and tungsten (W) can be used to grow a single crystal with a higher melting temperature than Ir [64–66]. On the other hand, carbon crucibles are widely used for producing single crystals of halides (fluoride, chloride, bromide, and iodide) from the viewpoint of reactivity with crucibles and prevention of oxidation of starting materials. Alumina ( $\alpha$ -Al<sub>2</sub>O<sub>3</sub>) and zirconia (ZrO<sub>2</sub>), which are chemically stable and do not easily volatilize and crack at high temperature, are generally used as the material of the ceramic crucible when a metal single crystal is grown.



**Figure 1.27** Schematic diagram and actual furnace of  $\mu$ -PD method for oxide single crystals.



**Figure 1.28** Crucibles for  $\mu$ -PD method, and schematic diagram and actual images around bottom of crucible during crystal growth. (a) Small and (b) large wetting angle between crucible and melt.

As mentioned above, there is a hole (capillary) in the bottom of the crucible, and the melt in the crucible passes through the capillary and reaches the bottom to form a meniscus when the melt has good wettability to the crucible material. This is the case where the wetting angle is small (Figure 1.28a). Specifically, in the case where an oxide single crystal is grown using a precious metal crucible such as Ir and Pt, the wettability between melt and crucible is good. On the other hand, when the wettability between the melt of starting materials and the crucible is poor (wetting angle

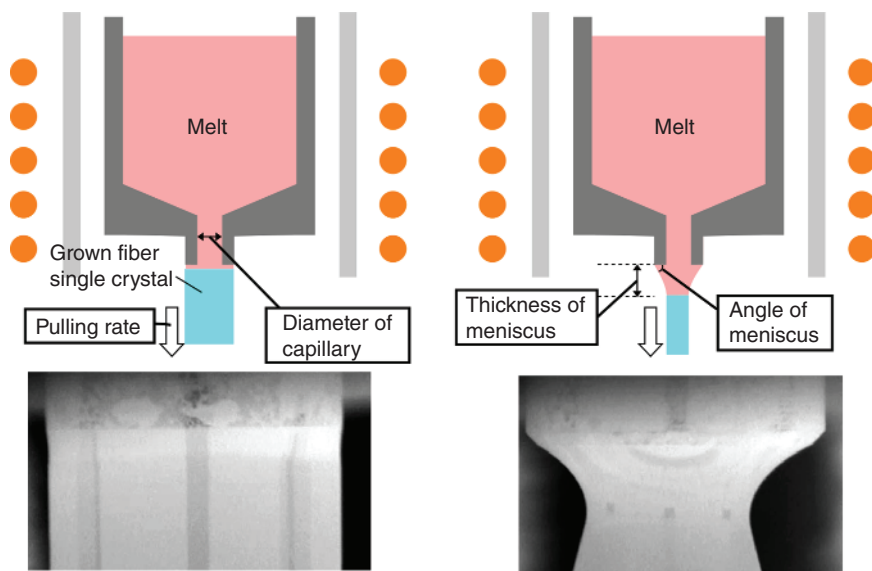


**Figure 1.29** Schematic diagrams of crystal growth with small and large thicknesses of meniscus by the  $\mu$ -PD method.

is large), the melt in the crucible doesn't pass through the capillary spontaneously. Therefore, the melt in the crucible is pulled down forcibly by a seed and a single crystal can be grown by adjusting the temperature gradient around the bottom of the crucible to form a solid-liquid interface in the capillary. In such cases, a single crystal rod has the same diameter as the hole in the capillary (Figure 1.28b). The wettability is poor in cases such as combination of the carbon crucible and the melt of fluoride or the ceramic crucible and the melt of metal.

**Segregation of  $\mu$ -PD Method** In the case of the  $\mu$ -PD method, size of capillary, thickness of meniscus, and diameter of the grown single crystal affect the segregation in the grown single crystal (Figure 1.29). Numerical simulation is an effective method to investigate the dopant distribution in the crystal growth, and some report about the numerical simulation for the  $\mu$ -PD method. The influencing factors on the radial dopant distribution included pulling velocity, the temperature profile of the die, and the height of meniscus. In the  $\mu$ -PD method with the characteristic radial segregation different from the Cz and BS methods, sufficient attention must be paid to the segregation not only in the growth direction but also in the radial direction when crystal growth of materials containing dopants whose segregation coefficient is far from 1.

In the previous report by Maier et al., both theoretical simulation and experiment showed that sapphire- and garnet-type single crystals with Cr, Yb, and Ga dopant ions grown by the  $\mu$ -PD method exhibited significantly different segregation states in the radial direction when the segregation coefficient is larger than 1 and when it is smaller than 1 [67]. In addition, Shimura calculated the radial distributions of dopants with various segregation coefficients in the  $\text{Y}_3\text{Al}_5\text{O}_{12}$  single crystal [68].

Rudolph et al. divided the area inside the capillary and the meniscus into Zones I and II, respectively, and investigated the effect of diameters of capillary and grown single crystal on the segregation in the growth direction [69]. Lan et al. calculated the Ge distribution in the  $\text{Ge}_x\text{Si}_{1-x}$  single crystal grown by the  $\mu$ -PD method using some parameters such as the thickness of meniscus, temperature of the die, growth rate, and diameter of the grown crystal [58].

In the case of the  $\mu$ -PD method using a metal crucible with a thin capillary, we need to be careful about the segregation in the radial direction perpendicular to the growth direction. Particularly in materials containing a dopant with small  $k_{\text{eff}}$  ( $<1$ ) such as the Ce-doped  $\text{Y}_3\text{Al}_5\text{O}_{12}$ , the dopant ( $\text{Ce}^{3+}$ ) may segregate around the periphery area. In the previous experimental and theoretical reports [70, 71], the size and number of the capillary at the die of the crucible greatly affect the segregation of dopant in the radial direction of a single crystal grown by the  $\mu$ -PD method when oxide single crystals are grown using a metal crucible with a small capillary. On the other hand, in the case of materials containing a dopant with large  $k_{\text{eff}}$  ( $>1$ ) such as the Cr-doped  $\text{Gd}_3\text{Ga}_5\text{O}_{12}$ , dopant ( $\text{Cr}^{3+}$ ) segregates around the capillary position in the radial direction of the single crystal grown by the  $\mu$ -PD method [72].

The segregation of dopant in the cross-section is due to the thin meniscus area between the bottom of the die and grown single crystal. In general, the thickness of the meniscus area is around 100–500  $\mu\text{m}$  during the crystal growth. As a result, the Marangoni convection occurs only around the outer periphery area in the meniscus. Unlike the Cz method, forced convection does not occur because the pull-down shaft and grown single crystal are not rotated, and the convection around the center area in the meniscus becomes insufficient. Therefore, when there is a capillary in the center of the die, the melt with the nominal composition is continuously supplied from the inside the crucible and the melt is transported as it is to the solid–liquid interface without sufficient mixing with the melt in the periphery area. Then, the nonuniformity of the meniscus appears as the segregation in the radial direction of the grown single crystal.

In the previous report [71], simulations were performed with changing the number of the capillaries, and the results showed that increasing the capillary number improves the segregation in the radial direction of the single crystal grown by the  $\mu$ -PD method. In addition, according to the results of the simulations,  $\text{Y}_3\text{Al}_5\text{O}_{12}:\text{Ce}$  and  $\text{Gd}_3(\text{Ga},\text{Al})_5\text{O}_{12}:\text{Ce}$  single crystals were grown using two- types of Ir crucibles with one or five capillaries, and the  $\text{Ce}^{3+}$  ion segregations in the radial direction of the grown single crystals were investigated [70]. Similar to the results of simulations, the increase in the number of capillaries improved the variation of dopant concentration around the capillary positions, resulting in improved uniformity in the radial direction of the grown single crystal. In addition, the improved uniformity of the dopant segregation has simultaneously enhanced optical and scintillation properties (Figure 1.30).

**Material Research by  $\mu$ -PD Method** One of the characteristics of the  $\mu$ -PD method is the higher growth rate compared to other melt-growth methods such as Cz and BS methods. Although it depends on the material, the  $\mu$ -PD method can generally grow

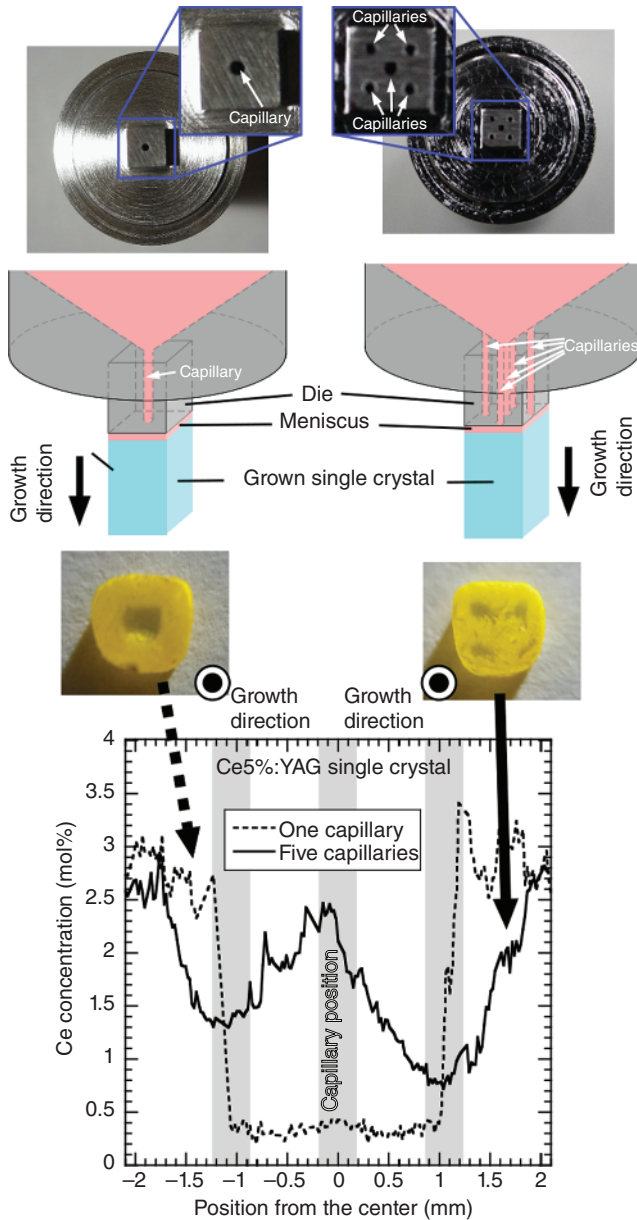


**Figure 1.30** Effect of number of capillaries on Ce segregation in YAG:Ce single crystals grown by  $\mu$ -PD method.

a single crystal several to 10 times faster than the Cz and BS methods. The high growth rate of the  $\mu$ -PD method is made possible by the small diameter of the grown crystal and the higher temperature gradient around the solid-liquid interface. In the melt-growth of the single crystal, supercooling is the driving force for growth. Therefore, it is necessary to eliminate the latent heat continuously when the melt



solidifies at the solid–liquid interface under the temperature gradient. Since the  $\mu$ -PD method grows a single crystal fiber with a diameter of several millimeter, the amount of latent heat that must be eliminated per unit time is relatively small even when the growth rate is high. In addition, the solid–liquid interface is formed at the bottom of the crucible and the temperature gradient can be increased easily compared to Cz and BS methods where the solid–liquid interface is formed above or in the crucible.

**Growth of Shape-Controlled Oxide Single Crystal by  $\mu$ -PD Method** Another feature of the  $\mu$ -PD method is that the shape-controlled single crystal can be grown because the single crystal is grown using a die of the crucible as shown in Figure 1.31a. Unlike the Cz and FZ methods, the shape of the meniscus on the bottom of the die in the  $\mu$ -PD method can be changed relatively freely, and a shape-controlled single crystal rod can be produced. In the previous reports, shape-controlled functional single crystals with various shapes have been grown by the  $\mu$ -PD method using specially designed crucibles for each shape (Figure 1.31b). In the case of good wetting (small wetting angle) such as oxide melt and noble crucibles, shape of the grown single crystal can be controlled by the shape of the meniscus just below the die of the crucible, and the shape of the meniscus is controlled by the bottom shape of the die. On the other hand, in the case of bad wetting (large wetting angle) such as fluoride melt and carbon crucible, the shape of the grown single crystal can be controlled by the shape of the capillary. Figure 1.31c shows the shape-controlled functional single crystals grown by the  $\mu$ -PD method. So far, single crystals with controlled shapes such as fiber, plate, square, columnar, and tubular have been grown directly from the melt in systems of oxide, fluoride, and metal materials [73–75].

**Growth of Shape-Controlled Fluoride Single Crystal by  $\mu$ -PD Method** In the case of shape-controlled fluoride single crystal, the specially designed carbon crucibles are used to control the shape of the solid–liquid interface during the crystal growth [76]. As I mentioned above, the wetting angle is large between the melt of fluoride material and the carbon crucible. Therefore, the shape control method for fluoride single crystals differs significantly from that for oxide single crystals. Specifically, shape of the melt is controlled by restricting the shape of the melt using a capillary at the bottom of crucible and a carbon product at the solid–liquid interface during the crystal growth to obtain the desired shape of the grown single crystal. Figure 1.32a shows a schematic diagram of crystal growth for tube-shaped fluoride single crystal by the  $\mu$ -PD method using a carbon crucible and the solid–liquid interface during the crystal growth of tube-shaped  $\text{CaF}_2$  single crystal. The outer shape can be controlled by the shape of the capillary in the carbon crucible, and if you want to grow a square-shaped single crystal rod, the capillary should be square in shape. On the other hand, the inner shape can be controlled by a carbon product such as a carbon rod attached to a carbon lid or pull-down shaft.

As shown in Figure 1.32b, two types of tube-shaped  $\text{CaF}_2$  single crystals were grown by the  $\mu$ -PD method using specially designed carbon crucibles [77]. The grown tube-shaped  $\text{CaF}_2$  single crystals have circular and square outer shapes.



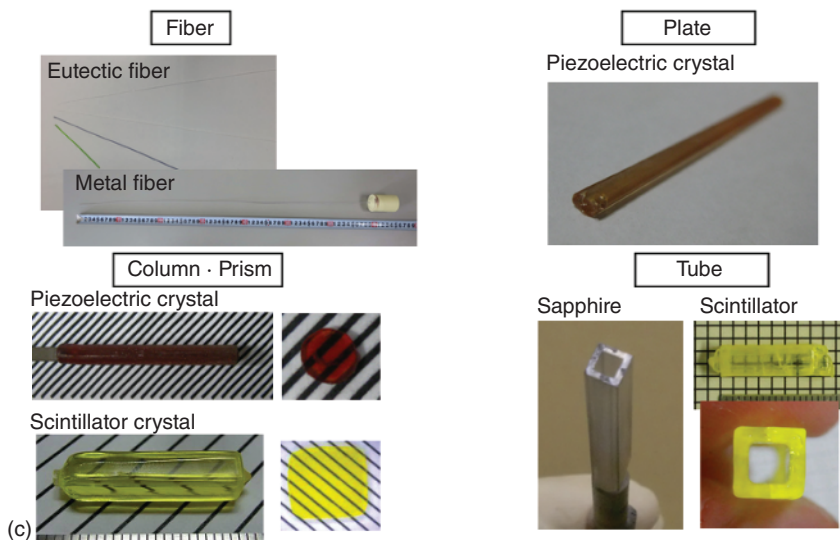
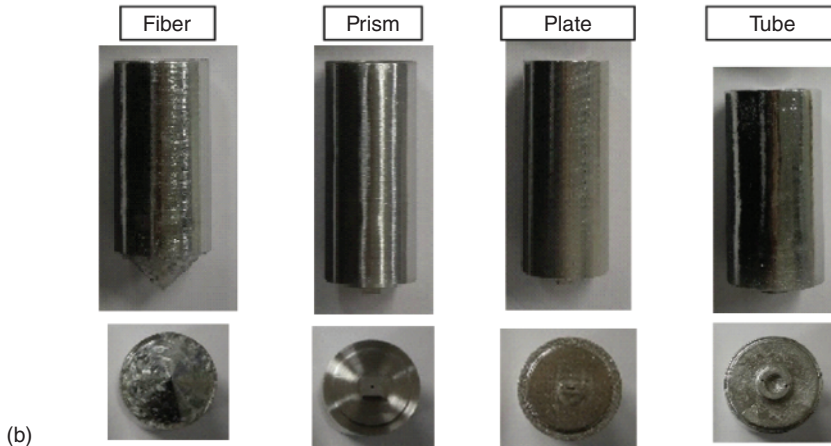
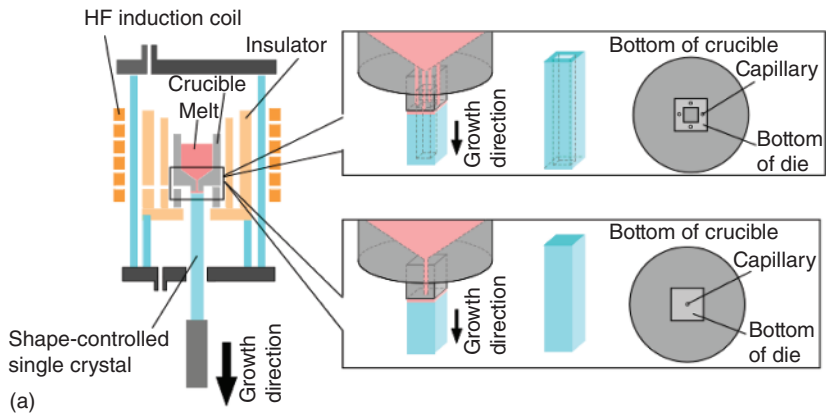


**Figure 1.31** (a) Schematic diagram of shape-controlled crystal growth by the  $\mu$ -PD method. (b) Crucibles for various shape-controlled crystal growths. (c) Shape-controlled functional single crystals grown by the  $\mu$ -PD method.

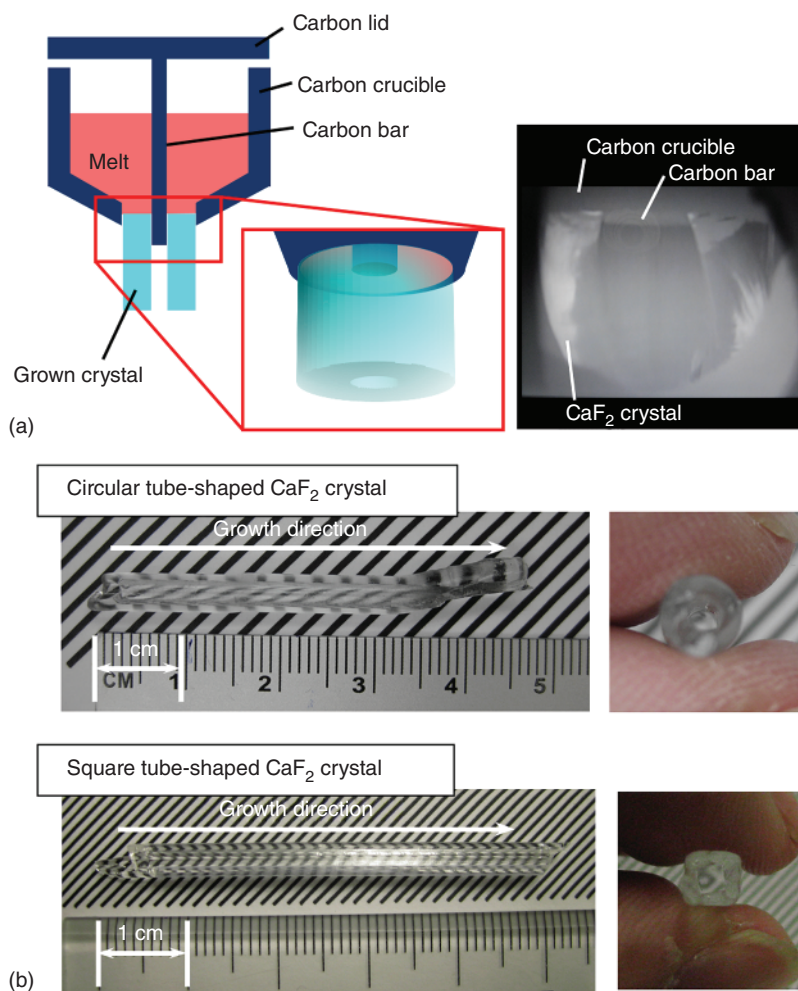


**Figure 1.32** (a) Schematic diagram of crystal growth for tube-shaped fluoride single crystal by the  $\mu$ -PD method and solid-liquid interface during the crystal growth of tube-shaped CaF<sub>2</sub> single crystal. (b) Two types of tube-shaped CaF<sub>2</sub> single crystals grown by  $\mu$ -PD method.

Inner diameters of the grown single crystals were controlled by the carbon rod attached to the carbon lid.

**A- $\mu$ -PD Method** In recent years, a novel technology developed by applying shape-controlled crystal growth to metals and alloys with poor workability has also begun to be used, and it is called “alloy-micro-pulling-down (A- $\mu$ -PD) method” [77–79]. Figure 1.33a shows a schematic diagram of the A- $\mu$ -PD method and the developed A- $\mu$ -PD furnace. Since melts of most metals and alloys exhibit bad wettability to ceramics crucibles, it is possible to fabricate metal and alloy fiber crystals with the same diameter as the capillary diameter of the crucible from the

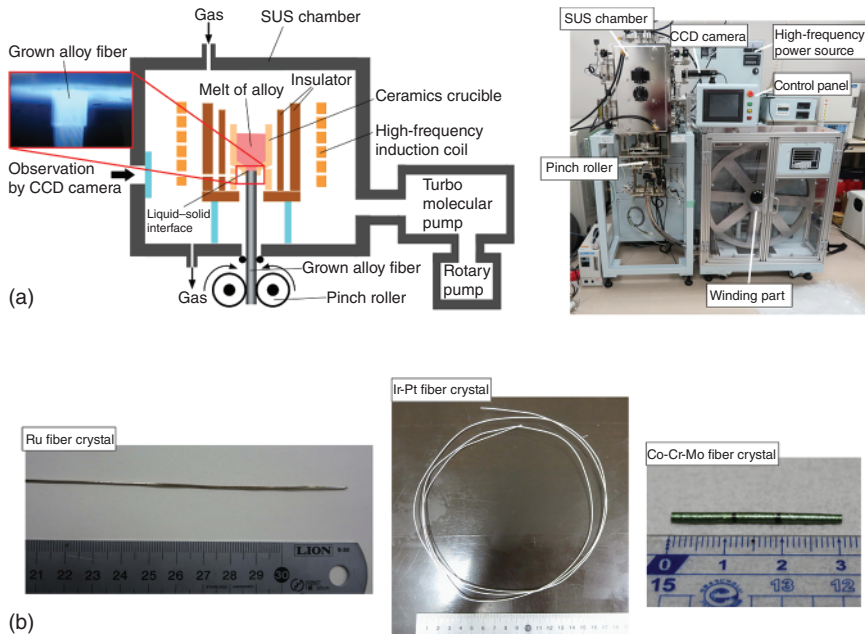


**Figure 1.33** (a) Schematic diagram of A- $\mu$ -PD method and developed A- $\mu$ -PD furnace. (b) Metal and alloy fiber crystals grown by A- $\mu$ -PD method.

melt directly. As a result of the development of a zirconia ceramic crucible with high mechanical strength and thermal shock resistance even at high temperatures around 2400 °C, iridium, platinum, ruthenium, and their alloy fiber crystals could be fabricated from the melt by the A- $\mu$ -PD method using a crucible as shown in Figure 1.33b [77, 78]. The A- $\mu$ -PD method is an effective technique for making fiber crystals from metals and alloys with poor workability other than precious metals, and has also succeeded in making fiber crystals from Co-Cr-Mo biomaterial alloys [79]. In addition, phase and mechanical properties of the Co-Cr-Mo fiber crystals fabricated by the A- $\mu$ -PD method could be controlled by the growth rate.

**Growth Process of  $\mu$ -PD Method** Figure 1.34 shows the flow chart of crystal growth using  $\mu$ -PD method. First, mixed starting materials are set into the crucible, and the crucible is heated by the high-frequency induction coil up to the melting point of the target material. After the starting materials were perfectly melted in the crucible, the melt comes out from the hole of the crucible by the capillary action in the case of an oxide melt in a metal crucible. The melt spreads on the bottom of the die, and the seed crystal is connected the melt. After sufficiently familiarizing the melt in contact with the seed crystal, pulling down a single crystal is started. During the crystal growth, the output of HF power supply and pulling-down rate are adjusted to keep the meniscus thickness at a few hundred  $\mu\text{m}$  thickness. When the crystal growth is finished, the cooling process is carried out.

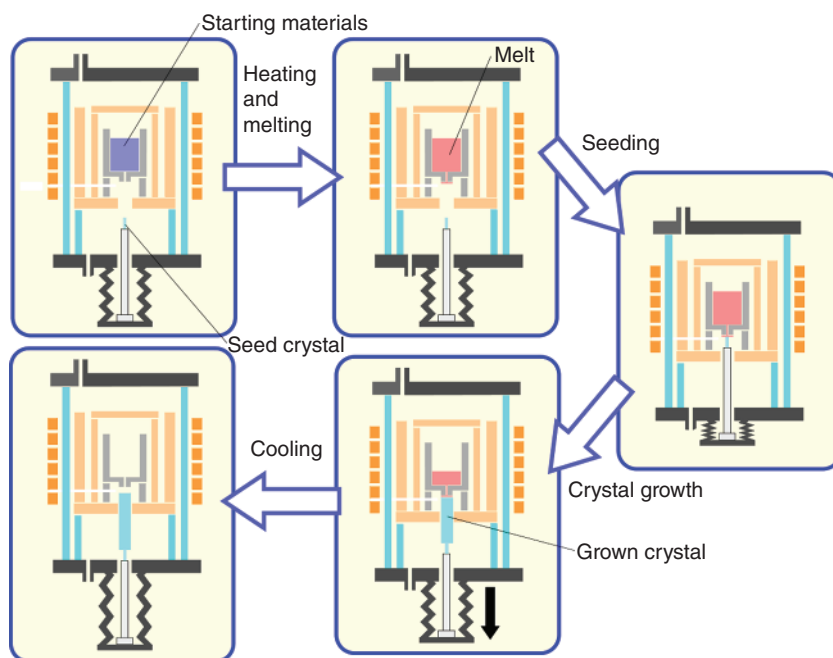


**Figure 1.34** Flow chart of crystal growth using  $\mu$ -PD method.

#### 1.2.3.5 Edge-Defined Film-Fed Growth Method

Edge-defined film-fed growth (EFG) method can grow a shape-controlled single crystal using a die from the melt in a crucible [80]. A schematic diagram of the EFG method is shown in Figure 1.35. A die with one or more capillaries is placed in the crucible. The melt passes through the capillary (capillaries) or slit (slits), and reaches the top of the die. The melt on the top of the die gets wet and spreads over the entire top surface of the die. By pulling-up the wet and spread melt using a seed crystal, a single crystal with the same cross-sectional shape as the upper surface of the die is continuously grown. As the die material, platinum, iridium, graphite, etc. are used, and  $\text{LiNbO}_3$ , sapphire, and Si single crystals are grown using the platinum, iridium, and graphite dies, respectively [81–83].

Like the  $\mu$ -PD method, shape-controlled single crystals could be grown by controlling the cross-sectional shape of the meniscus between the grown crystal and the die. There are some reports of growth for shape-controlled single crystals such as plate, tube, and complex shapes by the EFG method. Plate-shaped sapphire single crystals are mass produced by the EFG method.

As with the Cz method, the growth condition can be controlled by the shape and position of the crucible and insulators, the type and flow rate of atmosphere gas, the output of high-frequency induction power, etc. In addition, it is easy to obtain a large growth rate in the EFG method due to increasing the temperature gradient around top of the die. Recently, a plate-shaped  $\beta\text{-Ga}_2\text{O}_3$  single crystal was developed by the EFG method using Ir crucible and die with a slit [84].

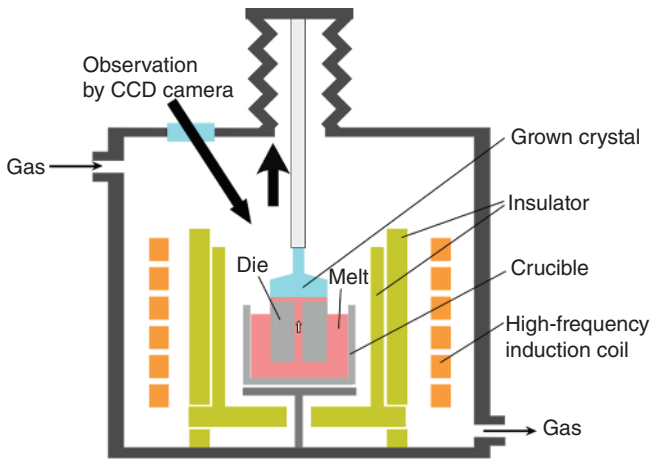


**Figure 1.35** Schematic diagram of EFG method.

#### 1.2.3.6 Verneuil Method

Verneuil method was developed by Auguste Victor Louis Verneuil in 1902 [85]. In the Verneuil method, powders of starting materials are made into droplets of the melt by passing them through the oxyhydrogen flame, and the droplets are accumulated to grow a large bulk single crystal with a round bar shape (Figure 1.36). Therefore, the Verneuil method is also known as the flame fusion method. Since it is possible to grow a single crystal in a short time while observing the growth conditions, the Verneuil method is suitable for mass production of large single crystals. It has been used for many years in the mass production of ruby and sapphire single crystals [86, 87]. However, the obtained single crystal often contains many oxygen defects and crystal defects such as the stacking fault and line defect due to effects of melting by the oxyhydrogen flame and crystal growth in a short time.

Starting materials are used in fine powder form, and they are filled into a container placed on top of the Verneuil furnace. Starting material powders in the container are fed into the lower heating area through the bottom hole of the container by vibration, and the supplied amount of starting material powders is controlled by the intensity and frequency of the vibration. The starting material powders move downward inside a thin tube along with oxygen and reach the thicker tube that is supplied with hydrogen. Ignition occurs at the point where oxygen and hydrogen meet and combustion occurs. The starting material powders melt in the oxyhydrogen flame and become droplets. The droplets fall on the seed crystal placed at the bottom of the furnace and crystallize at the top of the seed crystal.

#### 1.2.3.7 Laser-Heated Pedestal Growth Method

Laser-heated pedestal growth (LHPG) method is based on a laser heating zone melting method for single crystal fibers such as  $Y_2O_3$  and  $Sr_3Al_2O_6$  [88, 89] as illustrated in Figure 1.37. In addition, the laser heating floating zone method was developed for growth of single crystal fibers of sapphire, SiC, etc. [90]. According to the results of the zone melting method and the laser heating floating zone method, the LHPG

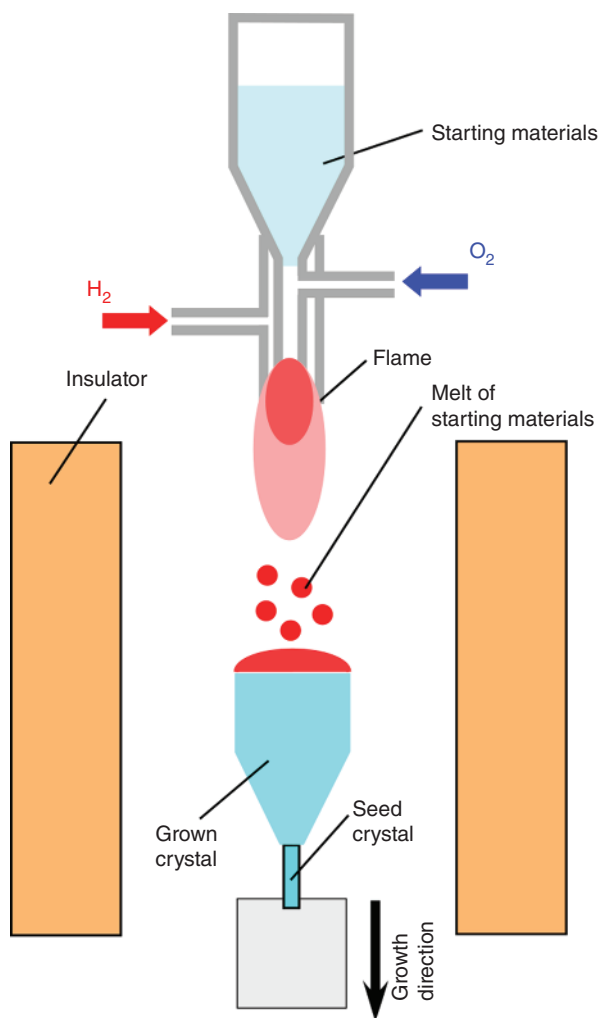


**Figure 1.36** Schematic diagram of Verneuil method.

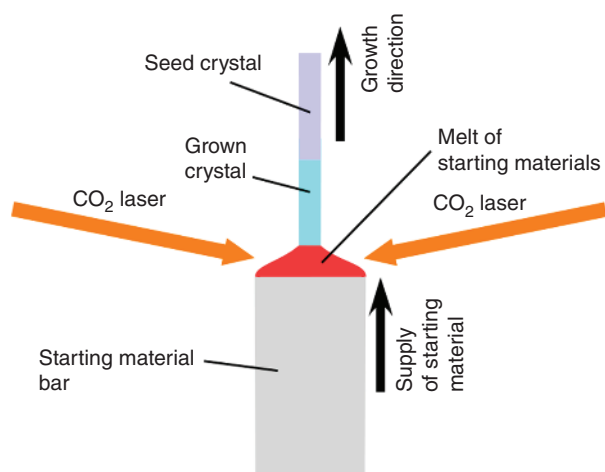


**Figure 1.37** Schematic diagram of LHPG method.

method using  $\text{CO}_2$  laser beam was developed and it is widely used in commercial LHPG furnace.  $\text{LiNbO}_3$  and vanadate ( $\text{Ca}_3\text{V}_2\text{O}_8$  and  $\text{SrVO}_3$ ) single crystal fibers as a nonlinear optical material were also grown by the LHPG method [91, 92]. The LHPG method has a relatively faster growth rate than other growth methods such as Cz and BS methods.

### 1.2.3.8 Skull Melting Method

Skull melting method can grow a single crystal with high melting point using a cold crucible using high frequency on the order of MHz [93, 94]. A schematic diagram of a typical skull melting furnace is shown in Figure 1.38. The high frequency makes it possible to directly heat the melt of starting materials. The periphery of the starting materials is cooled by a water-cooled copper pipe, and the cold crucible composed of starting materials is formed on the periphery. Since the skull melting method doesn't use a precious metal crucible such as iridium and platinum crucibles, there is no cost of the crucible, limitations of atmosphere and temperature by the crucible, and changes of growth conditions by deterioration and deformation of the crucible. They are big advantages in the mass production of functional single crystals.

The skull melting method has been used for mass production of a cubic  $\text{ZrO}_2$  single crystal with a melting point above  $2200^\circ\text{C}$  because there are no melting temperature limitations due to the usable temperature of the crucibles. However, it is difficult to control the flow of the melt in the cold crucible and the diameter of the grown single crystal by the output of the high-frequency oscillator, and the growth of a bulk single crystal without cracks using a seed crystal like the Cz method has not been performed. In order to carry out the unidirectional solidification, a method of crystallization by slowly moving the high-frequency induction coil downward relative to the starting material after melting the starting material is used.

In recent years, the development of crystal growth technology for large bulk single crystals based on the skull melting method has been carried out [95]. It is a method that enables pulling up a bulk single crystal like the Cz method by adding a pulling axis to the skull melting method, and it's called "oxide crystal growth from cold crucible (OCCC) method." The advantages of the OCCC method are that the crucible costs can be reduced and single crystals with high melting point can be grown

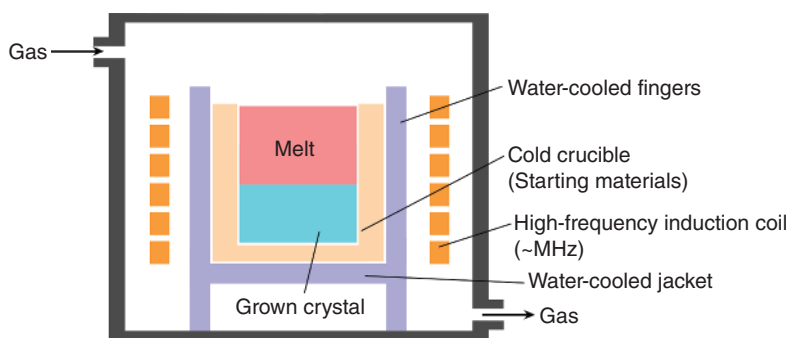


**Figure 1.38** Schematic diagram of skull melting method.



because crucibles are not used without the crucible temperature limit. In principle, single crystals with large diameter can be grown by the OCCC method since it is possible to pull a bulk single crystal with the suitable growth rate for crack-free and good crystallinity, and it is expected to be a next-generation mass production technology with low-cost performance.

### 1.2.3.9 Top-Seeded Solution Growth Method

In contrast to melt-growth methods such as Cz, BS, and FZ, growing single crystals from a solution is called the solution-growth method. Among the solution-growth methods, growing single crystals by immersing a seed crystal in the upper part of the solution is called the top-seeded solution growth (TSSG) method (Figure 1.39) [96]. The TSSG method can grow a large size of single crystals, and it has been used for the mass production for bulk single crystals of various incongruent melting materials such as  $\text{BaTiO}_3$ ,  $\text{KTaO}_3$ , and  $\text{CsLiB}_6\text{O}_{10}$  (CLBO) [97–99].

In the TSSG method, crystal growth proceeds at the same position by holding the seed crystal above the crucible. In particular, even crystals with a high specific gravity can be grown without sinking to the bottom of the crucible, making it possible to increase the size of the crystal. Continuous transport of solute components by the natural convection occurs above the solution in the crucible. As a result, a large crystal can be grown, although it takes a longer time to grow than the melt-growth methods. Clear crystal planes appear in the crystal grown by the TSSG method as is the case with many solution-growth methods. The TSSG method that doesn't pull up the seed crystal is called Kyropoulos (Ky) method, and the Ky method has been used for mass production of sapphire single crystals [100]. On the other hand, in the case of crystal growth in a concentrated solution system, the single crystal may be grown while being pulled up the seed crystal at a low speed because of the relatively high growth rate. The TSSG method that pulls up the seed crystal is called Cz-type TSSG

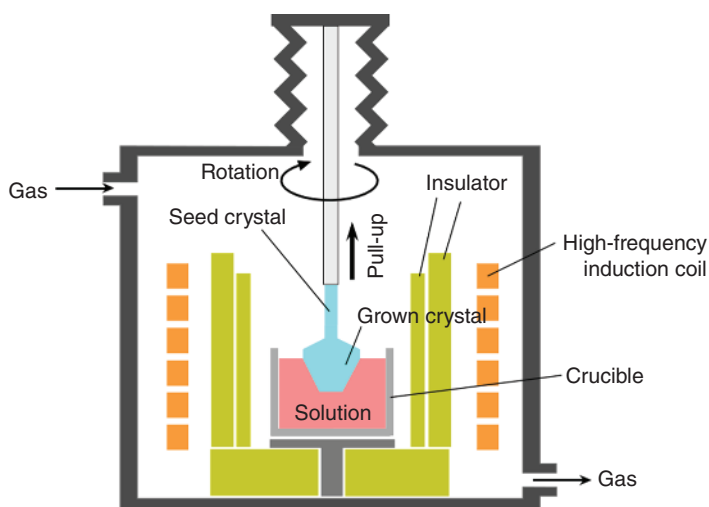


**Figure 1.39** Schematic diagram of TSSG method.

method or TSSG-pulling method. There are two types of TSSG furnaces: resistance heating-type and high-frequency induction heating-type furnaces. The resistance heating-type TSSG furnace can easily control temperature distribution in the vertical direction by adjusting the crucible position and output of heater. Therefore, for the Ky-type TSSG method, the resistance heating-type furnace is suitable because convection can be easily controlled. On the other hand, it is easy to create a horizontal temperature gradient because the crucible is heated directly by high frequency in the high-frequency induction heating-type furnace. As a result, in the Cz-type TSSG method using the high-frequency induction heating-type furnace, it is easy to control the diameter of the grown single crystal during crystal growth while pulling. Therefore, it is important to properly use the furnace according to the purpose in order to obtain a high-quality single crystal.

#### 1.2.3.10 Arc Melting

The arc melting furnace has been used to melt metals and alloys using the arc discharge. Metals and alloys with high melting point can be melted relatively easily by the arc melting furnace. As illustrated in Figure 1.40, the arc melting furnace is generally composed of a vacuum-tight chamber, pump, water-cooled copper hearth, arc electrode, electrode operation arm, observation window, and flip arms. First, melting of a sample is started by the heat coming from the arc generated between the electrode and the water-cooled copper hearth. As melting of the sample progresses, the arc is generated between the electrode and the molten sample in the water-cooled copper hearth.

There are some reports about the material research with high melting point using the arc melting furnace. The “core heating (CH) method” has been developed as a novel growth method for the research of materials with higher melting point than Ir [101, 102]. The CH method uses metals such as Ir with high melting point and low reactivity, and the metals heated by the arc are the heating source in the CH method. As a result, unlike the Cz and BS methods, target materials can be melted without using a crucible. The short growth time of inorganic materials with high melting point can be achieved using the arc melting system while it is difficult to control the growth direction and grow a single crystal with high crystallinity. Therefore, it is suitable for efficient evaluations of phase formation and properties as an initial stage of material research.

In addition, the “shielded arc melting (SAM) method” is also proposed as a novel crystal growth method using the arc melting for materials with high melting point and high volatility [103]. In the SAM method, starting materials on the water-cooling Cu hearth are covered and surrounded by Ta or W plates with higher melting point than Ir, and the Ta(W) plates are heated by the electrical arc. As a result, the high-speed crystal growth of the inorganic materials with high melting point and high volatility is also able to be achieved without a crucible by the radiant heating from the Ta(W) plates. In the previous report [103], the  $\text{Zn}_3\text{Ta}_2\text{O}_8$  crystal was grown by the SAM method and the scintillation properties were investigated. However, there are many cracks in the  $\text{Zn}_3\text{Ta}_2\text{O}_8$  crystal growth by the SAM method, and the size of transparent grain is approximately 0.5 mm.

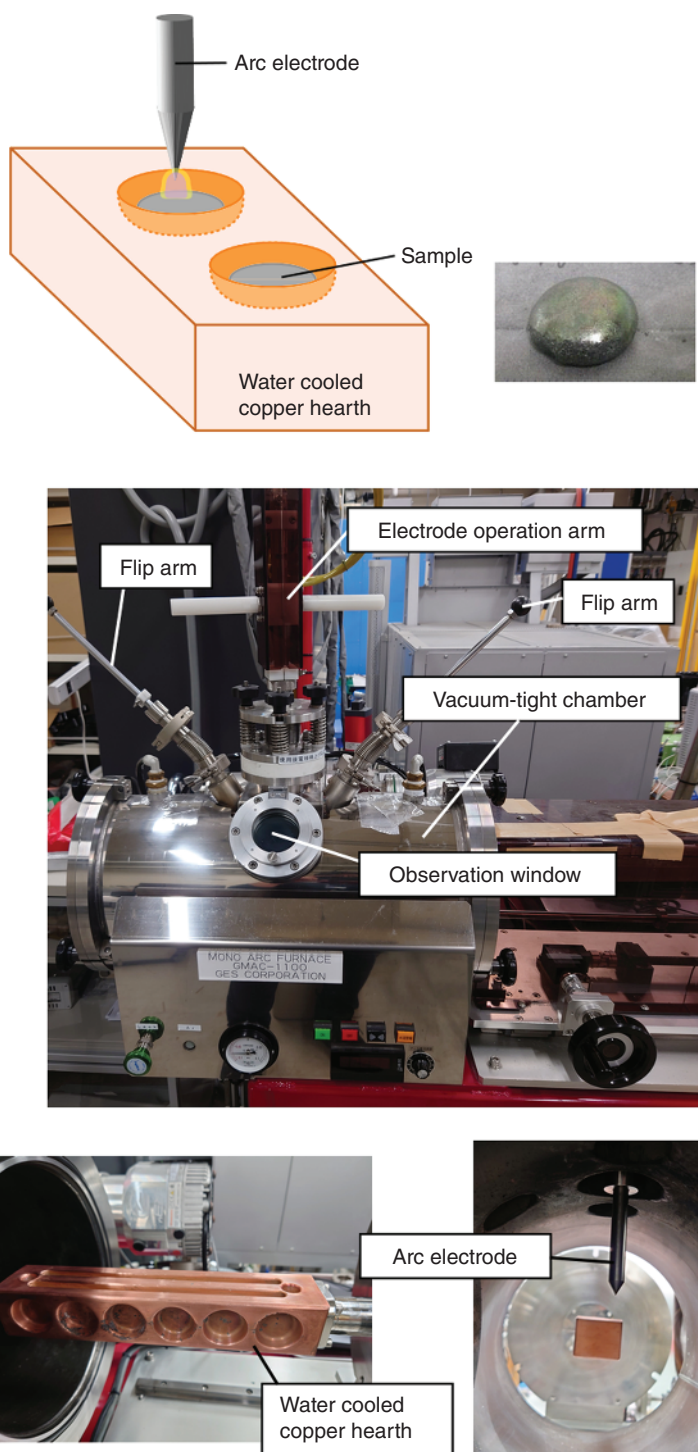


Figure 1.40 Schematic diagram and actual furnace of arc melting method.

Although these growth methods are still in the development stage and it is difficult to grow high-quality single crystals, future progress is expected because they enable efficient material research that cannot be achieved by the conventional growth methods.

#### 1.2.3.11 Heat-Exchange Method

The heat-exchange method (HEM) has been developed for crystal growth of sapphire and spinel-type  $\text{MgAl}_2\text{O}_4$  single crystals as a gradient furnace technique [104–106]. Large bulk single crystal can be grown by the HEM using a large crucible, although the crystallinity is lower than crystals grown by the Cz and BS methods. As shown in Figure 1.41, crystal growth is performed from the interface between melt and seed crystal by gradual cooling after the starting materials and portion of the seed crystal are melted by the heating. The heat exchanger causes the seed and grown single crystal to be slightly lower in temperature than the melt, so that the crystal growth proceeds while extracting heat from them. However, it is difficult to control shape and moving speed of the solid–liquid interface during the crystal growth, and as a result, the grown single crystal tends to contain vacancies and defects.

Figure 1.42 shows the crystal growth method of fluoride and halide single crystals using the HEM. Initially, a single crystal fiber is pulled down from the capillary at the bottom of the crucible using a seed crystal and wire as in the general  $\mu$ -PD method. After confirming that the single crystal fiber without cracks has been pulled down, stop pulling down the single crystal fiber. Then, the heating of the crucible is gradually lowered to the grown bulk single crystal inside the crucible from the grown single crystal fiber at the bottom of the crucible. In this method, the grown single crystal fiber serves as the heat exchanger and seed crystal.

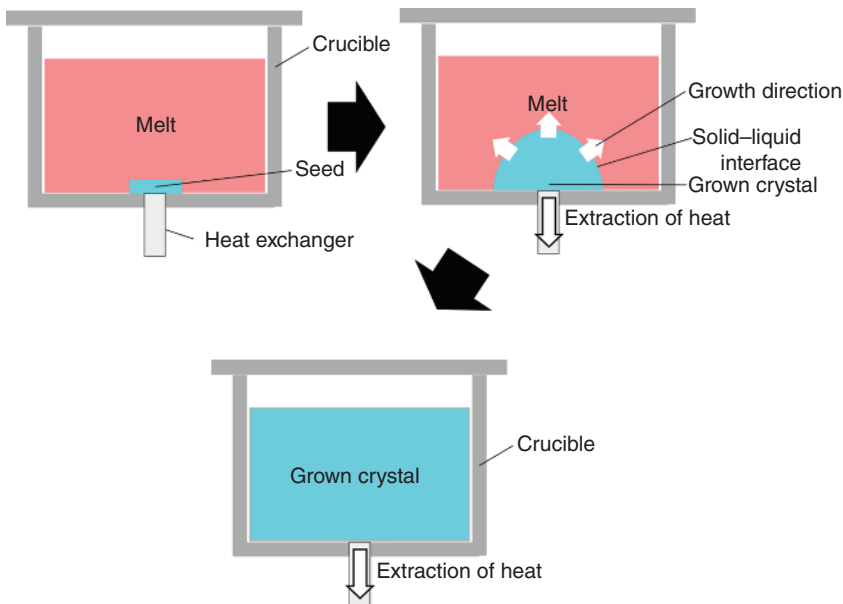


**Figure 1.41** Schematic diagram of heat-exchange method.

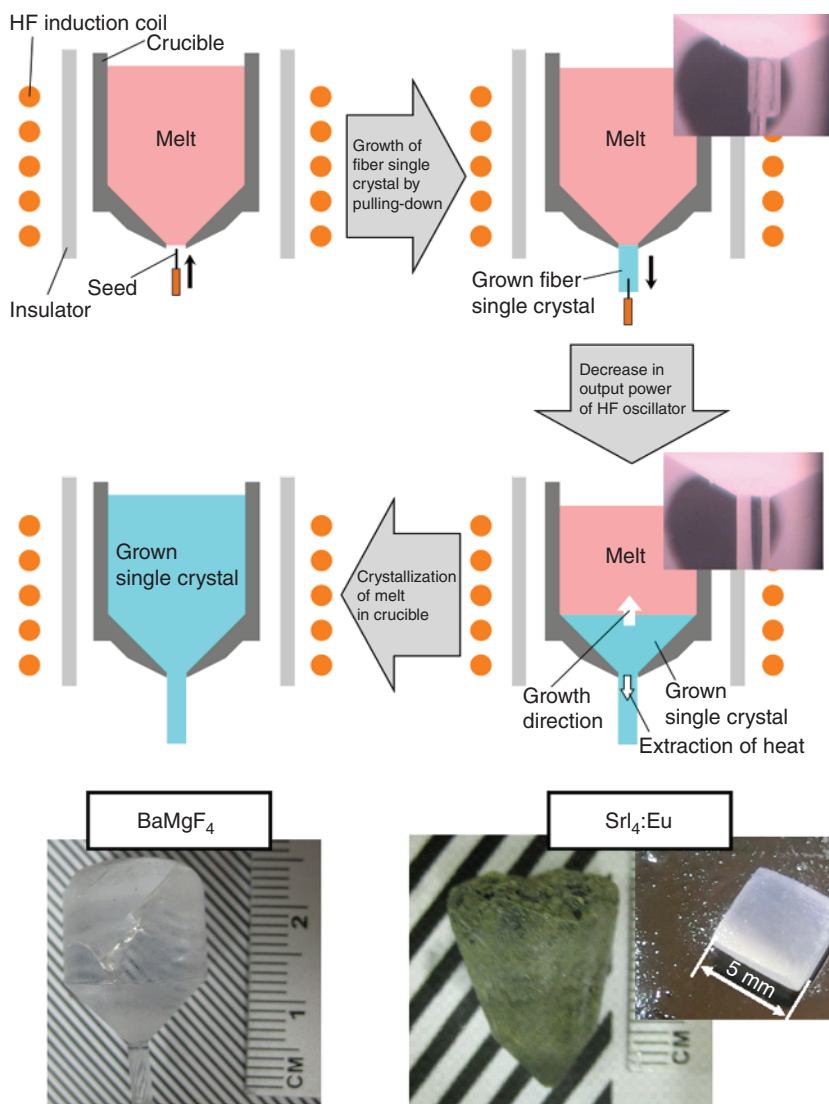


**Figure 1.42** Schematic diagram of crystal growth method integrating  $\mu$ -PD method and HEM, and BaMgF<sub>4</sub> and SrI<sub>2</sub>:Eu single crystal grown by the method.

## References

- 1 Hofstadter, R. (1978). *Phys. Rev.* 74: 100.
- 2 Lecoq, P., Gektin, A., and Korzhik, M. (2017). *Inorganic Scintillator for Detector Systems*, 408. Springer.
- 3 Moszynski, M., Ludziejewski, T., Wolski, D. et al. (1994). *Nucl. Inst. Methods Phys. Res. A* 345: 461.
- 4 Ogino, H., Yoshikawa, A., Nikl, M. et al. (2006). *J. Cryst. Growth* 287: 335.

- 5 Moszynski, M., Kapusta, M., Wolski, D. et al. (1998). *Nucl. Inst. Methods Phys. Res. A* 404: 157.
- 6 Lempicki, A., Randles, M.H., Wisniewski, D. et al. (1995). *IEEE Trans. Nucl. Sci.* 42: 280.
- 7 Melcher, C.L. and Schweitzer, J.S. (1992). *Nucl. Inst. Methods Phys. Res. A* 314: 212.
- 8 Weber, M.J. (2004). *Nucl. Inst. Methods Phys. Res. A* 527: 9.
- 9 Takagi, K. and Fukazawa, T. (1983). *Appl. Phys. Lett.* 42: 43.
- 10 Weber, M.J. and Monchamp, R.R. (1973). *J. Appl. Phys.* 44: 5496.
- 11 Moszynski, M., Balcerzyk, M., Kapusta, M. et al. (2005). *IEEE Trans. Nucl. Sci.* 52: 3124.
- 12 Lecoq, P., Dafinei, I., Auffray, E. et al. (1995). *Nucl. Instrum.* 365: 291.
- 13 Shah, K.S., Glodo, J., Klugerman, M. et al. (2003). *IEEE Trans. Nucl. Sci.* 50: 2410.
- 14 Higgins, W.M., Churilov, A., van Loef, E. et al. (2008). *J. Cryst. Growth* 310: 2085.
- 15 Cherepy, N.J., Hull, G., Drobshoff, A.D. et al. (2008). *Appl. Phys. Lett.* 92: 083508.
- 16 Burger, A., Rowe, E., Groza, M. et al. (2015). *Appl. Phys. Lett.* 107: 143505.
- 17 Combes, C.M., Dorenbos, P., van Eijk, C.W.E. et al. (1999). *J. Lumin.* 82: 299.
- 18 Zhuravleva, M., Blalock, B., Yang, K. et al. (2012). *J. Cryst. Growth* 352: 115.
- 19 Zhuravleva, M., Yang, K., and Melcher, C.L. (2011). *J. Cryst. Growth* 318: 809.
- 20 Pfann, W.G. (1957). *Solid State Physics*, 4e. New York: Academic Press.
- 21 Burton, J.A., Prim, R.C., and Schlichter, W.P. (1987). *J. Chem. Phys.* 1958: 21.
- 22 Mori, M., Xu, J., Okada, G. et al. (2016). *J. Ceram. Soc. Jpn.* 124: 569.
- 23 Chen, C., Brennecka, G.L., Synowicki, R.A. et al. (2018). *J. Am. Ceram. Soc.* 101: 3797.
- 24 Wang, Z., Zhou, G., Jiang, D., and Wang, S. (2018). *J. Adv. Ceram.* 7: 289.
- 25 Zorenko, Y., Mares, J.A., Prusa, P. et al. (2010). *Radiat. Meas.* 45: 389.
- 26 Luo, L., Dietze, M., Solterbeck, C.H. et al. (2013). *J. Appl. Phys.* 114: 224112.
- 27 Muñoz-García, A.B., Artacho, E., and Seijo, L. (2009). *Phys. Rev. B* 80: 014105.
- 28 Zorenko, Y., Voloshinovskii, A., Savchyn, V. et al. (2007). *Phys. Status Solidi B* 244: 2180.
- 29 Sekiya, T., Yagisawa, T., Kamiya, N. et al. (2004). *J. Phys. Soc. Jpn.* 73: 703.
- 30 Yokota, Y., Fujimoto, Y., Yanagida, T. et al. (2011). *Cryst. Growth Des.* 11: 4775.
- 31 Czochralski, J. and Phys, Z. (1917). *Chem.* 92: 219.
- 32 Wu, Y., Koschan, M., Foster, C., and Melcher, C.L. (2009). *Cryst. Growth Des.* 19: 4081.
- 33 Kamada, K., Yanagida, T., Endo, T. et al. (2012). *J. Cryst. Growth* 352: 91.
- 34 Latynina, A., Watanabe, M., Inomata, D. et al. (2013). *J. Alloys Compd.* 553: 89.
- 35 Yokota, Y., Ohashi, Y., Kudo, T. et al. (2017). *J. Cryst. Growth* 468: 321.
- 36 Yokota, Y., Ohashi, Y., Kudo, T. et al. (2015). *Jpn. J. Appl. Phys.* 54: 10–13.
- 37 Nguyen, T.P. and Chen, J. (2019). *Int. J. Heat Mass Transf.* 130: 1307.
- 38 Miyazawa, S. (1980). *J. Cryst. Growth* 49: 515.
- 39 Carruthers, J.R. (1976). *J. Cryst. Growth* 32: 13.



- 40 Carruthers, J.R. (1976). *J. Cryst. Growth* 36: 212.
- 41 Bridgman, P.W. (1925). *Proc. Am. Acad. Arts Sci.* 60: 305.
- 42 Stockbarger, D.C. (1926). *Rev. Sci. Instrum.* 7: 133.
- 43 Blum, S.E. and Chicotka, J. (1973). *J. Electrochem. Soc.* 120: 588.
- 44 Hoshikawa, K., Osada, J., Saitou, Y. et al. (2014). *J. Cryst. Growth* 395: 80.
- 45 Kimura, S. and Kitamura, K. (1992). *J. Am. Ceram. Soc.* 75: 1440.
- 46 Balbashov, A.M. and Egorov, S.K. (1981). *J. Cryst. Growth* 52: 498.
- 47 Duffar, T. (2010). *Crystal Growth Processes Based on Capillarity*. Wiley.
- 48 Kravtsov, A. (2018). *IOP Conf. Ser.: Mater. Sci. Eng.* 355: 012007.
- 49 Khpayeh, S.M., Fort, D., and Abell, J.S. (2008). *Prog. Cryst. Growth Charact. Mater.* 54: 121.
- 50 Yokota, Y., Shimoyama, J., Ogata, T. et al. (2007). *Solid State Commun.* 142: 429.
- 51 Watauchi, S., Matsuya, K., Nagao, M. et al. (2017). *J. Cryst. Growth* 468: 465.
- 52 Zajíc, F., Klejch, M., Eliáš, A. et al. (2023). *Cryst. Growth Des.* 23: 2609.
- 53 Ito, T., Ushiyama, T., Yanagigawa, Y. et al. (2013). *J. Cryst. Growth* 363: 264.
- 54 Ammerahl, U., Dhalenne, G., Revcolevschi, A. et al. (1998). *J. Cryst. Growth* 193: 55.
- 55 Nishimura, Y., Matsuoka, Y., Miyashita, S. et al. (1999). *J. Cryst. Growth* 207: 206.
- 56 Ali, M.S., Sato, N., Fukasawa, I. et al. (2019). *Cryst. Growth Des.* 19: 6291.
- 57 Yoon, D.-H. and Fukuda, T. (1994). *J. Cryst. Growth* 144: 201.
- 58 Lan, C.W., Uda, S., and Fukuda, T. (1998). *J. Cryst. Growth* 193: 552.
- 59 Shimamura, K., Uda, S., Yamada, T. et al. (1996). *Jpn. J. Appl. Phys.* 35: L793.
- 60 Jung, I.H., Lee, J.H., Yang, W.J. et al. (2002). *Mater. Lett.* 56: 1069.
- 61 Yoshikawa, A. and Chani, V. (2009). *MRS Bull.* 34: 266.
- 62 Fukuda, T. and Chani, V.I. (2007). *Shaped Crystals: Growth by Micro-Pull-and-Down Technique*. Springer.
- 63 Yokota, Y., Yoshikawa, A., Futami, Y. et al. (2012). *IEEE Trans. Ultrason. Ferroelectr. Freq. Control* 59: 1868.
- 64 Fukabori, A., Chani, V., Kamada, K. et al. (2011). *J. Cryst. Growth* 318: 823.
- 65 Yoshino, M., Kotaki, A., Yokota, Y. et al. (2022). *CrystEngComm* 12: 1215.
- 66 Suda, T., Yokota, Y., Horiai, T. et al. (2022). *J. Cryst. Growth* 583: 126547.
- 67 Maier, D., Rhede, D., Bertram, R. et al. (2007). *Opt. Mater.* 30.
- 68 Simura, R., Yoshikawa, A., and Uda, S. (2009). *J. Cryst. Growth* 311: 4763.
- 69 Rudolph, P. and Fukuda, T. (1999). *Cryst. Res. Technol.* 34: 3.
- 70 Yokota, Y., Kudo, T., Ohashi, Y. et al. (2017). *J. Mater. Sci. Mater. Electron.* 28: 7151.
- 71 Zeng, Z., Qiao, L., Liu, Y. et al. (2016). *J. Cryst. Growth* 434: 110.
- 72 Matsukura, D., Kurosawa, S., Yamaji, A. et al. (2024). *J. Cryst. Growth* 630: 127581.
- 73 Yokota, Y., Kurosawa, S., Ohashi, Y. et al. (2016). *J. Cryst. Growth* 452: 69.
- 74 Yokota, Y., Sato, M., Chani, V. et al. (2013). *Sens. Actuator A Phys.* 200: 56.
- 75 Kotaki, A., Yoshino, M., Yokota, Y. et al. (2020). *Appl. Phys. Express* 13: 125503.
- 76 Yokota, Y., Tanaka, H., Sato, M. et al. (2011). *MRS Online Proc. Libr.* 1309: 1013090629.



- 77 Yokota, Y., Nihei, T., Tanaka, K. et al. (2018). *Adv. Eng. Mater.* 20: 1700506.
- 78 Nihei, T., Yokota, Y., Arakawa, M. et al. (2017). *J. Cryst. Growth* 468: 403–406.
- 79 Yokota, Y., Nihei, T., Abe, S., and Yoshikawa, A. (2021). *Adv. Eng. Mater.* 23: 2100144.
- 80 LaBelle, H.E. Jr. (1971). *Mater. Res. Bull.* 6: 581.
- 81 Fukuda, T. and Hirano, H. (1975). *Mater. Res. Bull.* 10: 801.
- 82 Chalmers, B., LaBelle, H.E. Jr., and Mlavsky, A.I. (1972). *J. Cryst. Growth* 13: 84.
- 83 Ciszek, T.F. (1972). *Mater. Res. Bull.* 7: 731.
- 84 Kuramata, A., Koshi, K., Watanabe, S. et al. (2016). *Jpn. J. Appl. Phys.* 55: 1202A2.
- 85 Verneuil, A.V. (1902). *Compt. Rend.* 135: 791.
- 86 Ueltzen, M. (1993). *J. Cryst. Growth* 132: 315.
- 87 Kurlov, V.N. (2001). *Encyclopedia of Materials: Science and Technology*, 2e, 8259. Elsevier.
- 88 Goutaudier, C., Ermenieux, F.S., Cohen-Adad, M.T., and Moncorge, R. (2000). *J. Cryst. Growth* 210: 693.
- 89 Fernández-Carrión, A.J., Bourret, J., Sharp, J. et al. (2022). *Cryst. Growth Des.* 22: 6828.
- 90 Feigelson, R.S. (1986). *J. Cryst. Growth* 79: 669.
- 91 Chen, C., Chen, J., and Chia, C. (2007). *Opt. Mater.* 30: 393.
- 92 Ardila, D.R., Andreetta, J.P., Ribeiro, C.T.M., and Li, M.S. (1999). *Rev. Sci. Instrum.* 70: 4606.
- 93 Osiko, V.V., Borik, M.A., and Lomonova, E.E. (1987). *Annu. Rev. Mater. Sci.* 17: 101.
- 94 Michel, D., Perez, M., Jorba, Y., and Collongues, R. (1978). *J. Cryst. Growth* 43: 546.
- 95 Yoshikawa, A., Kochurikhin, V.V., Tomida, T. et al. (2024). *Sci. Rep.* 14: 14881.
- 96 Miller, C.E. (1958). *J. Appl. Phys.* 29: 233.
- 97 Wemple, S.H., Didomenico, M. Jr., and Camlibel, I. (1968). *J. Phys. Chem. Solids* 29: 1797.
- 98 Whipps, P.W. (1972). *J. Cryst. Growth* 12: 120.
- 99 Mori, Y., Kuroda, I., Nakajima, S. et al. (1995). *J. Crystal Growth* 156: 307.
- 100 Hu, K.Y., Xu, J., Wang, C.Y. et al. (2012). *J. Inorg. Mater.* 27: 1321.
- 101 Kurashima, Y., Kurosawa, S., Murakami, R. et al. (2021). *Cryst. Growth Des.* 21: 572.
- 102 Ishizawa, S., Kurosawa, S., Kurashima, Y. et al. (2023). *Opt. Mater.* 142: 113941.
- 103 Yajima, R., Kamada, K., Takizawa, Y. et al. (2022). *Opt. Mater.: X* 14: 100149.
- 104 Schmid, F. and Viechnicki, D. (1970). *J. Am. Ceram. Soc.* 53: 528.
- 105 Viechnicki, D. and Schmid, F. (1971). *J. Cryst. Growth* 11: 345.
- 106 Viechnicki, D., Schmid, F., and McCauley, J.W. (1972). *J. Appl. Phys.* 43: 4508.

